

Aminopyrazine Inhibitors Binding to an Unusual Inactive Conformation of the Mitotic Kinase Nek2: SAR and Structural Characterization[†]

Daniel K. Whelligan,[‡] Savade Solanki,[‡] Dawn Taylor,[‡] Douglas W. Thomson,[‡] Kwai-Ming J. Cheung,[‡] Kathy Boxall,[‡] Corine Mas-Droux,[§] Caterina Barillari,^{§,||} Samantha Burns,[‡] Charles G. Grummitt,[§] Ian Collins,[‡] Rob L. M. van Montfort,^{§,||} G. Wynne Aherne,[‡] Richard Bayliss,[§] and Swen Hoelder^{*,‡}

[‡]Cancer Research UK Cancer Therapeutics Unit, The Institute of Cancer Research, 15 Cotswold Road, Sutton, Surrey SM2 5NG, United Kingdom, [§]Chester Beatty Laboratories, Section of Structural Biology, The Institute of Cancer Research, 237 Fulham Road, London SW3 6JB, United Kingdom, and ^{||}Haddow Laboratories, Section of Cancer Therapeutics, The Institute of Cancer Research, Sutton, Surrey SM2 5NG, United Kingdom

Received July 13, 2010

We report herein the first systematic exploration of inhibitors of the mitotic kinase Nek2. Starting from HTS hit aminopyrazine **2**, compounds with improved activity were identified using structure-based design. Our structural biology investigations reveal two notable observations. First, **2** and related compounds bind to an unusual, inactive conformation of the kinase which to the best of our knowledge has not been reported for other types of kinase inhibitors. Second, a phenylalanine residue at the center of the ATP pocket strongly affects the ability of the inhibitor to bind to the protein. The implications of these observations are discussed, and the work described here defines key features for potent and selective Nek2 inhibition, which will aid the identification of more advanced inhibitors of Nek2.

Introduction

Nek2 is a serine/threonine kinase that plays a key role in cell division. It localizes to the centrosome and regulates spindle pole organization and separation through phosphorylation of substrates including C-Nap1, rootletin, and Nlp.^{a,1–5} In addition to its centrosomal role, Nek2 has also been implicated in chromatin condensation through phosphorylation of HMGA2 and spindle checkpoint control through interaction with or phosphorylation of Hec1, Mad1, and Mad2.^{6,7} Nek2 expression and activity are tightly regulated in a cell cycle-dependent manner. Expression levels are low in G1 and increased in S/G2.⁸ Following mitotic entry Nek2 is targeted for proteasomal degradation by the APC/C.⁹ Though Nek2 dimerizes and is rapidly activated by autophosphorylation, it is kept in the inactive form through dephosphorylation by protein phosphatase 1 (PP1) until PP1 is inhibited through binding of inhibitor-2 and phosphorylation by Nek2.¹⁰

[†]Atomic coordinates and structure factors for the crystal structures of ligand bound Nek2 can be accessed using the following PDB codes: **2** (2XKF), **12** (2XKD), **14** (2XKC), **15** (2XK8), **17** (2XK4), **23** (2XK7), **35** (2XK3), and **36** (2XK6).

*To whom correspondence should be addressed. Phone: +44 20 87224353. Fax: +44 2087224047. Email: swen.hoelder@icr.ac.uk.

^aAbbreviations: ADP, adenosine diphosphate; APC/C, anaphase-promoting complex/cyclosome; ATP, adenosine triphosphate; BINAP, 2,2'-bis(diphenylphosphino)-1,1'-binaphthyl; Chk, checkpoint kinase; DCE, dichloroethane; DIPEA, *N,N*-diisopropylethylamine; DME, dimethoxyethane; DMF, dimethylformamide; Hec1, high expression in cancer-1; HMGA2, high-mobility group AT-hook 2; HTS, high-throughput screening; Mad, mitotic arrest deficient-like; Nap1, nucleosome assembly protein-1; NBS, *N*-bromosuccinimide; Nek, (never in mitosis gene a)-related kinase; NIMA, never in mitosis gene a; Nlp, ninein-like protein; NMP, *N*-methylpyrrolidone; PAMPA, passive membrane permeability assay; Plk, polo-like kinase; PMB, *p*-methoxybenzyl; SAR, structure–activity relationship; SD, standard deviation; TFA, trifluoroacetic acid; THF, tetrahydrofuran; TPSA, topological polar surface area.

Several recent reports suggest that Nek2 is abnormally expressed in cancer cells, and experimental studies have suggested that Nek2 expression contributes to the classic tumor hallmarks of aneuploidy and chromosome instability.¹¹ Overexpression of Nek2 leads to premature centrosome separation and the accumulation of cells with multiple nuclei and supernumerary centrosomes.^{12,13} Recent studies suggest that RNAi depletion of Nek2 leads to antiproliferative effects, e.g., in HeLa cells¹⁴ and cholangiocarcinoma cell lines.¹⁵ RNAi depletion of Nek2 reduced tumor size and peritoneal dissemination of cholangiocarcinoma tumor xenografts in immunosuppressed mice.¹⁵ Similarly, genetic knockdown of Nek2 resulted in an antiproliferative and antimigratory phenotype in MDA-MB-231 breast cancer cells and an antitumor effect in a MDA-MB-231 xenograft model when the silencing oligonucleotides were injected intratumorally.¹⁶ Intriguingly, depletion of Nek2 also synergized with cisplatin in inhibiting growth of colorectal cancer cells in vitro and in vivo, although the mechanism for this remains unclear.¹⁷ Taken together, these findings suggest Nek2 as a promising anticancer target.

Although a small molecule inhibitor of the interaction of Hec1 with Nek2 has been described¹⁸ and a Plk1 inhibitor **1** has been shown to have Nek2 activity in a counterscreen (Figure 1),¹⁹ no systematic investigation of Nek2 inhibitors has been disclosed to our knowledge. We herein report the exploration of a series of pyrazine-based Nek2 inhibitors identified through high-throughput screening (HTS).

Results and Discussion

Identification of initial hit compounds was achieved by a high-throughput biochemical screen²⁰ which furnished pyrazine **2** with an IC₅₀ of 0.87 μM (Figure 1). The compound showed a good overall profile, but we were concerned about

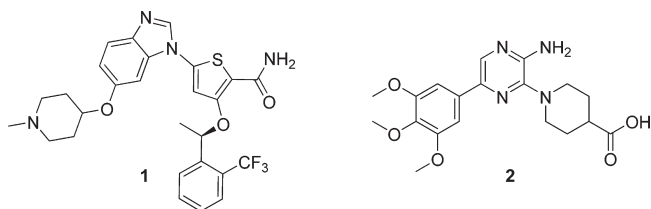
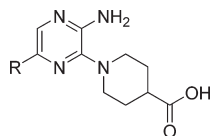


Figure 1. Structures of Plk1 inhibitor **1** demonstrating Nek2 activity in counterscreen and HTS hit **2**.

Table 1. Effect of Modification of the 5-(3,4,5)-Trimethoxyphenyl Ring of Inhibitor **2**^a



Compound	R	Nek2 IC ₅₀ (μ M)	TPSA (\AA^2)	PAMPA pH 5 / 7.4 (10^{-6} cm/s)	LE ^d
2		0.87 \pm 0.34	120.03	3.1 / 0.0	0.30
3		1.9 \pm 0.7	110.8	-	0.30
4		1.9 \pm 0.6	110.8	20.8 / 0.0	0.30
5		4.2 (3.9, 4.5)	101.57	51.5 / 0.0	0.31
6		19.8	101.57	-	0.27
7		7.8 (6.9, 8.6)	92.34	59.4 / 0.0	0.32
8	H	48.5	92.34	-	0.37

^aLigand efficiency, calculated according to ref 21. ^bResults are the mean (\pm SD) for $n \geq 3$ or the mean values of two independent determinations with individual determinations in parentheses or samples run at $n = 1$.

its low estimated membrane permeability (PAMPA and CACO-2 assays) and modest ligand efficiency (binding energy per heavy atom as described by Hopkins and co-workers)²¹ (Table 1).

We explored structural modifications around **2** to investigate how the potency, ligand efficiency, and permeability could be improved. The low permeability of **2** at physiological pH was attributed to the carboxylic acid group that predominantly exists as the carboxylate at this pH. However, the observation that permeation remained low at pH 5 in the passive membrane permeability assay (PAMPA) suggested that other

properties contributed to the low permeability, since a significantly larger fraction of the compounds should be protonated under these conditions. We focused our attention on the relatively high topological polar surface area (TPSA, Table 1) of **2**, since it has recently been suggested that polar surface area is a reasonable predictor for bioavailability and permeability of acids.²²

We therefore began with the removal of the methoxy groups from the 5-(3,4,5)-trimethoxyphenyl ring as they collectively represent 23% of the TPSA of **2**. Deletion of one methoxy group led to small drops in activity (**3** and **4**) (Table 1). Monomethoxy compound **5**, where substitution is meta to the pyrazine ring, was 4-5-fold less potent, and removal of both meta **6** or all methoxy groups **7** resulted in a significant loss of affinity when compared to hit **2**. Complete erasure of the phenyl group **8** affected an approximately 50-fold drop in activity.

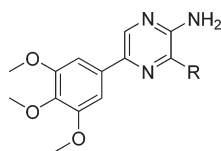
Compounds **4** and **5** were assessed for PAMPA, since they represented the best compromise between TPSA and Nek2 potency at this stage. Both compounds showed significantly increased permeability at pH 5 but still low permeability at physiological pH (Table 1). This suggests that TPSA is predictive for permeation at pH 5 when the carboxylic acid is protonated to an extent. We reasoned that good permeability at pH 5 could be sufficient for reasonable bioavailability through diffusion from the stomach or duodenum where the pH is significantly lower than 7.4.

Attention was next focused upon the piperidine ring, and a number of analogues were prepared (Table 2). Any modification of the carboxylic acid, e.g., removal **9** or replacement with the ester **10**, resulted in significant loss of activity, and only the primary amide **11** retained some potency.

Having identified the carboxylic acid as a key pharmacophoric point for activity, we decided to replace the piperidine ring by a phenyl ring, since this offered the advantage of easy modification. Though the corresponding benzoic acid **12** was slightly less potent than the HTS hit **2**, this result prompted preparation of substituted benzoic acid derivatives. Addition of a meta-methyl group **13** conferred a sharp decrease in inhibition, while having a methyl **14** or methoxy **15** group in the ortho position was tolerated. However, even slightly larger groups (ethyl instead of methyl **16** and ethoxy instead of methoxy **17**) were not tolerated, suggesting that it was not viable to improve potency by adding larger groups ortho to the carboxylic acid.

Our exploration of the SAR so far had shown that the carboxylic acid is critical for activity and the piperidine ring can be replaced by phenyl but attempts to improve potency by substitution of the benzoic acid were not successful. In order to guide further optimization, the crystal structures of compounds **2**, **5**, and **12** in the Nek2 catalytic domain were solved. These structures shared many common features with our recently reported crystal structure of Nek2.²³

The aminopyrazine ring forms two hydrogen bonds with the hinge region of Nek2, reminiscent of other well-known kinase inhibitors.^{24,25} The trimethoxyphenyl group lies coplanar at the entrance of the ATP pocket between the hinge region and the Gly-rich loop (Figure 2a). The contribution this group has to the potency is explained by the observation that the phenyl ring is engaging in hydrophobic contacts with Ile14 and Gly92 in Nek2. Interestingly the single methoxy group of **5** is unambiguously positioned above Gly91 and Gly92 (data not shown). Its small but significant effect on activity might be rationalized by more extensive polar interactions with the hinge, or exclusion of water molecules.

Table 2. Effect of Piperidine/Benzoic Acid Modification of Inhibitor **2**^b

Compound	R	Nek2 IC ₅₀ (μ M)	TPSA (\AA^2)	LE ^a
9		> 50	82.73	-
10		18.3	109.03	0.22
11		5.7 (5.3, 6.1)	125.82	0.26
12		2.3 \pm 0.5	116.79	0.28
13		> 50	116.79	-
14		2.6 \pm 0.5	116.79	0.26
15		2.4 \pm 0.5	126.02	0.26
16		26.2	116.79	0.21
17		16.9	126.02	0.21

^aLigand efficiency, calculated according to ref 21. ^bResults are the mean (\pm SD) for $n \geq 3$ or the mean values of two independent determinations with individual determinations in parentheses or samples run at $n = 1$.

The piperidine ring of **2** and **5** and the phenyl ring of the benzoic acid moiety of **12** is sandwiched between the gatekeeper residue Met86 and Phe148 (Figure 2a). The carboxylic acid group of compounds **2**, **5**, and **12** participates in a number of interactions, including hydrogen bonds with Tyr70 and Asp159 and a salt bridge with the catalytic lysine (Lys37) (Figure 2b and Figure 2c).

The Tyr70 residue is remarkable for two reasons: first, it is rare among kinases for Tyr to be present in this position,²³ and second, it shows an unusual conformation in the structures with **2**, **5**, and **12**. This conformation, which we have referred to as “Tyr-down”, has so far only been observed for Nek2 bound to inhibitors of this class and apo or ADP-bound Nek7.²³ The fact that the Tyr-down conformation is not observed with apo Nek2 or Nek2 bound to other types of inhibitors suggests an induced fit of the binding site by the class of inhibitors described here. The movement is induced through interactions between the inhibitor and the protein, in particular through the hydrogen bond of the carboxylate to Tyr70 but also through hydrophobic contacts with the Met gatekeeper. As shown in Figure 3, upon compound binding, Met86 and Leu59 adopt different positions than in the structures of Nek2 bound to nucleotides²⁶ and form a pocket that is occupied by Tyr70 in the tyrosine down conformation. The implication of the Tyr down conformation will be discussed below.

The crystal structures revealed another unusual feature of Nek2: the presence of a Phe (Phe148) at the base of the ATP pocket. Only 39 of human kinase catalytic domains contain a Phe in this position which is usually occupied by Leu in most kinases.²⁷ The larger Phe has a profound influence on the shape of the ATP pocket. It protrudes into the adenine sub-pocket creating steric hindrance in the plane of the hinge binding motif. As a result, the piperidine ring of **2** and the phenyl ring of the benzoic acid moiety of **12** rotate out of the plane of the aminopyrazine (50° for the benzoic acid).

This observation also explains why meta substituted benzoic acid derivative **13** is significantly less potent. The 50° rotation of the phenyl ring inevitably results in a steric clash of the meta substituents with Cys22 on one side or Val68 on the other side of the catalytic pocket. Also, meta substituents are going to favor an orthogonal disposition between the pyrazine and benzoic acid rings, and this is not well tolerated in the Nek2 active site because of the large Phe residue.

The cocrystal structures of **14**, **15**, and **17** with Nek2 were also solved in an attempt to explain the loss of activity with slightly larger alkyl groups (methoxy in **15** and ethoxy in **17**) (Figure 2). The benzoic acid ring of **14** was slightly shifted with respect to **12** away from Tyr70. Also the Tyr70 residue was observed in both up and down positions in the crystal structure, indicating that the side chain is mobile in this complex. The methyl group of compound **14** points toward the back of the catalytic pocket, in the direction of the hydroxyl group of Tyr70 in the Tyr-down conformation (Figure 2d).

Surprisingly, the binding mode of **15** represented an intermediate between **12** and **14**, with the phenyl ring occupying a position similar to **14** but with Tyr70 in only the down conformation (Figure 2e). The distance between the carboxylic acid group of the **15** and the hydroxyl group of Tyr70 was 4 \AA and thus too far to be a hydrogen bond (Figure 2e). The methoxy group fits compactly in the back of the pocket and makes contacts with Val68 and Tyr70. This explains why larger groups cannot be accommodated and perhaps why the Tyr-down conformation was observed with this compound, even though the hydrogen bond to Tyr70 is not formed. We also solved the cocrystal structure of **17**, which shows that the ethoxy group points toward the Gly-rich loop and thus confirms the hypothesis that this group is too large to be accommodated in the same position as the methoxy group of **15** (Figure 2f). The same argument might apply to ethyl substituted **16** which is significantly less active than **14** and **15**,

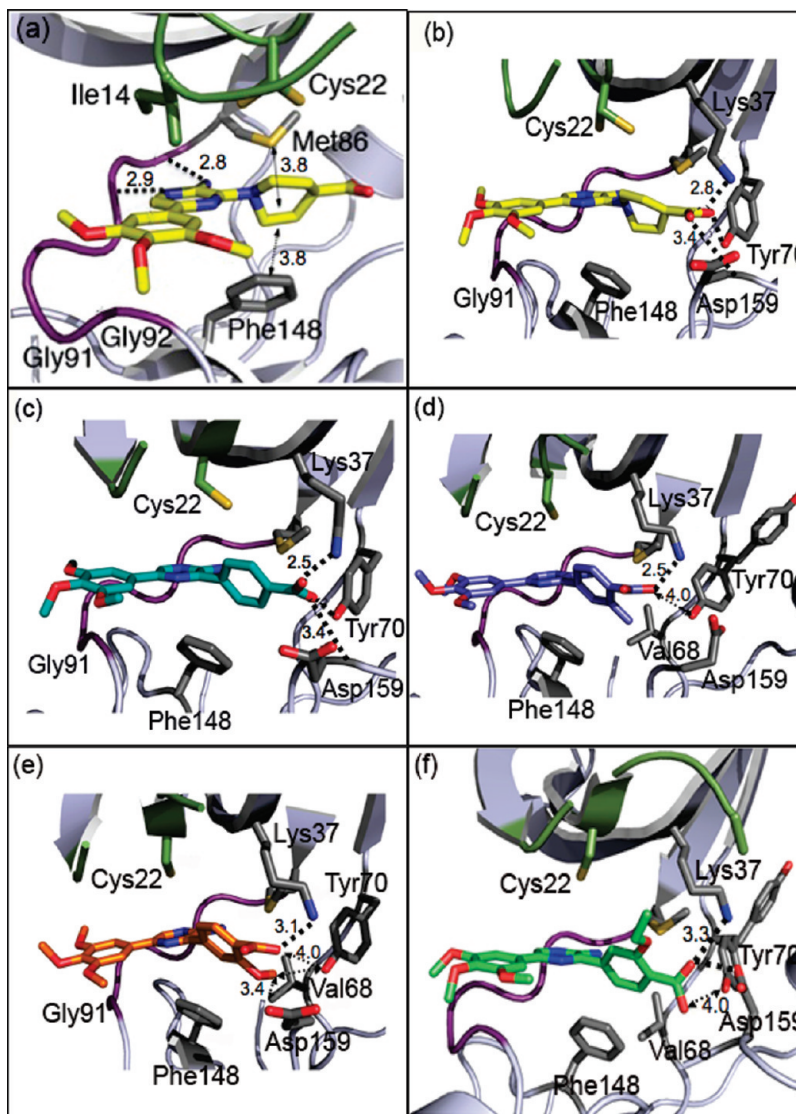


Figure 2. Binding mode of pyrazine inhibitors in Nek2 catalytic pocket. (a) Compound **2** (C in yellow): The trimethoxyphenyl group is located between Ile14 of the Gly-rich loop (green) and Gly91–Gly92 of the hinge region (purple). The piperidine ring is sandwiched between Phe148 and the gatekeeper residue Met86. The aminopyrazine ring forms two hydrogen bonds with the hinge region. Compounds **2** (b) and **12** (c) (C in cyan): The carboxylic acid interacts with Tyr70, Lys37, and Asp159. For substitutions of the phenyl ring, the methyl group of **14** (d) (C in lavender) and methoxy group of **15** (e) (C in orange) show differing effects on the Tyr70 conformation. In contrast with **14** and **15**, a larger substituent, the ethoxy group of compound **17** (f) (C in mint), points toward the Gly-rich loop. Residues Cys22 in (a) and (b) and Tyr70 in (d) and (f) are depicted with alternative conformations. Modifications on the piperidine ring do not have any effect on the remaining interactions with Nek2. All distances are in Å.

but the exact reason is difficult to rationalize as potential detrimental interactions between the ethyl group of **16** and the Tyr70 side chain or Val68 cannot be excluded.

The potency (IC_{50} values) of compounds **13**, **16**, and **17** coupled with the available cocrystal structures suggested that substitution of the benzoic acid moiety leads to steric repulsion invoked by Phe148 induced 50° rotation of the phenyl ring. As mentioned above, Phe is a rare and large residue in this position and has a profound influence on the shape of the ATP pocket. This and the large gate keeper (Met86) induce strong geometric constraints. As a result, only limited space remains for additional interactions between the inhibitor and the kinase, posing a significant challenge to improve affinity.

Only three other kinases with a Phe in this position have been crystallized with inhibitors (Braf, Wee1, and Plk1). A particularly relevant example to Nek2 is Plk1, which features not only a relatively large Leu gate keeper but also a Cys in the

position equivalent to that of Cys22 in Nek2. (Figure 2). Interestingly, the relevance of the equivalent Phe (Ph183 in Plk1) for inhibitor binding has recently been described.^{28,29}

We analyzed the available cocrystal structures of Plk1 in order to gain insights into how activity in our series can be improved. A pertinent example was the cocrystal structure of Plk1 with BI-2536 (**18**) (Figure 4). This inhibitor engages in a hydrophobic interaction with the Phe 183 comparable to our inhibitors with Phe148 in Nek2.²⁸ In addition, a derivative of **18** has been described to show significant activity against Nek2.²⁸

This structure offered some inspiration as to how additional potency against Nek2 can be derived: two alkyl groups, a cyclopentyl group and an ethyl group, of **18** reach into the region to the side of and behind Phe183 (corresponding to Phe148 in Nek2), respectively (Figure 4a). These groups engage in hydrophobic interactions with the kinase, very likely contributing to activity.²⁸ We reasoned that it should be possible to mirror

these interactions on Nek2 due to the sequence similarity with Plk1 in this region of the kinase.

As reported above, substituted benzoic acids did not improve activity. However, substitution of the phenyl group is only possible in the plane of the aromatic ring and this potentially results in a steric clash with Cys22. On the other hand, the sp^3 centers of the piperidine ring of compound **2** offered the possibility of placing substitution at a different angle relative to the ring.

We thus explored substitution of the piperidine of **2** starting with the racemic cis and trans methyl substituted compounds **19** and **22** (Table 3). While trans-substitution led to a small drop in activity, cis-substitution was equipotent to **2**. Extending from methyl to ethyl (**23** and **24**) resulted in a small loss of activity in the cis case and a significant loss in the trans case.

Since cis-substitution was preferred, additional substituted piperidines were prepared. Disappointingly, groups larger than ethyl led to an even larger loss of inhibition (**25** and **26**).

As the cis ethyl group was the largest group still tolerated, the crystal structure was solved after soaking Nek2 with racemic **23** (Figure 4b). Interestingly, only the *R,R* enantiomer

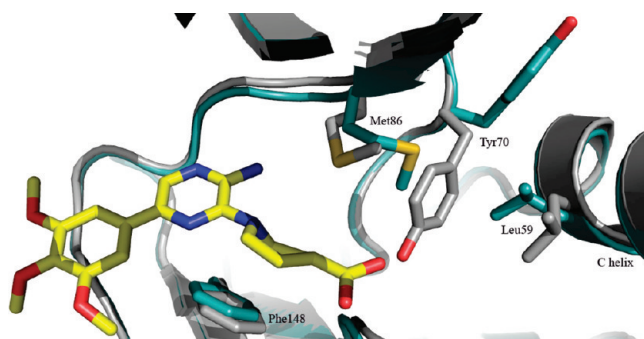


Figure 3. Opening of the Tyr70-down pocket by movement of Met86 upon inhibitor binding to Nek2. Tyr70-down conformation observed in Nek2 inhibitor-bound structure (gray) is sandwiched between Met86 “gatekeeper” and Leu59 of the C-helix. Compound **2** C is in yellow, and nucleotide bound Nek2 structure (PDB code 2W5H) is in teal.

could be mapped to the electron density, suggesting that this enantiomer is significantly more active than the other enantiomer. The ethyl group points upward toward Cys22, and the piperidine maintains a slightly different conformation compared to **2**. The side chain of Cys22, which adopts two conformations in **2**, has shifted to a single conformation creating a small pocket that accommodates the ethyl group analogous with Cys67 in the cocrystal structure of Plk1 with **18**.²⁸ The crystal structure of **23** also offered an explanation why **25** and **26** were significantly less active: the larger *n*-propyl and cyclopropyl groups very likely clash with Cys22.

The two enantiomers of **19** were separated by chiral HPLC. As expected, they showed very different inhibition. Enantiomer (–)-**20** was 10× less potent than the HTS hit **2**, while enantiomer (+)-**21** gave an IC_{50} of $0.39 \pm 0.18 \mu\text{M}$ ($n = 4$). The absolute stereochemistry of this enantiomer was not assigned. However, the observation that only the *R,R* enantiomer was observed in the crystals structure of ethyl substituted **23** suggests that the more active (+) enantiomer **21** features the same *R,R* stereochemistry. The slightly enhanced activity provided by the methyl group in **21** may be the result of an improved balance between additional beneficial hydrophobic contacts and repulsive interactions.

Superimposition of compound **23** with the above-mentioned structure of **18** bound to Plk1 indeed showed that the ethyl groups of the two compounds aligned closely (Figure 4b). Furthermore, the comparison suggested that substitution of an equatorial proton of the piperidine ring of inhibitor **19** or **23** by an alkyl group could mimic the cyclopentyl group of the Plk1 inhibitor **18**, leading to improved affinity. This equatorial position translates into the cis isomer with respect to the carboxylic acid, and we thus prepared a small series of compounds with hydrophobic groups attached to the 2-position (cis) of the piperidine ring.

While the racemic mixtures of compounds **27** and **28** gave comparable potency, propyl derivatives **29** and **30** led to a significant loss of activity. This loss could be explained by intramolecular steric repulsion between the alkyl groups and the pyrazine ring in the bioactive conformation resulting in a

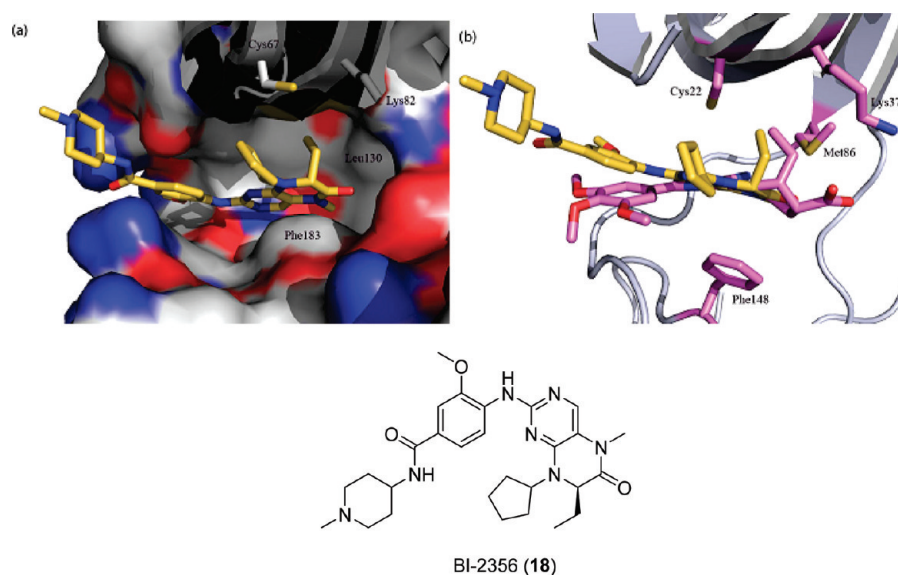
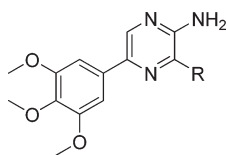
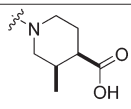
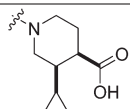
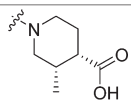
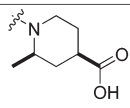
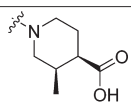
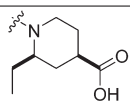
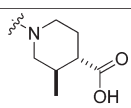
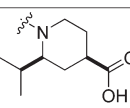
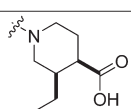
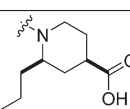
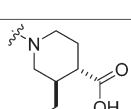
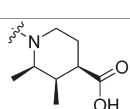
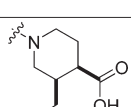
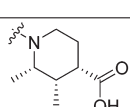


Figure 4. (a) Binding of BI-2536 (**18**) inhibitor (C in light yellow) to Plk1 (PDB code 2RKU). The ethyl group of BI-2536 is located in a small pocket between residues Cys67 (Cys22 in Nek2), Lys82 (Lys37 in Nek2), and the gatekeeper Leu130 (Met86 in Nek2). (b) Crystal structure of BI-2536 in Plk1 superimposed with the cocrystal structure of **23** in Nek2. Ethyl group of **23** and BI-2536 (**18**) point toward the same small pocket into the kinase catalytic site.

Table 3. Effect of Addition of Alkyl Groups to the Piperidine Ring of Inhibitor **2**^b

Compound	R	Nek2 IC ₅₀ (μ M)	LE ^a	Compound	R	Nek2 IC ₅₀ (μ M)	LE ^a
19	 (\pm)	0.72 (0.54, 0.90)	0.29	26	 (\pm)	38.3	0.20
20	 (-)	10.8	0.24	27	 (\pm)	1.2	0.28
21	 (+)	0.39 \pm 0.18	0.30	28	 (\pm)	1.4	0.27
22	 (\pm)	2.7	0.26	29	 (\pm)	5.9	0.23
23	 (\pm)	1.5	0.27	30	 (\pm)	5.4	0.23
24	 (\pm)	11.3	0.23	31	 (-)	0.23 (0.19, 0.26)	0.30
25	 (\pm)	11.2	0.22	32	 (+)	3.4	0.25

^aLigand efficiency, calculated according to ref 21. ^bResults are the mean (\pm SD) for $n \geq 3$ or the mean values of two independent determinations with individual determinations in parentheses or samples run at $n = 1$.

penalty to adopt this conformation. The Plk1 inhibitor **18** is rigid, and no penalty is incurred in this case.

Alternatively, a steric clash between the propyl groups of **29** and **30** and Phe148 might lead to a reduced IC₅₀ despite additional hydrophobic contacts. In any case, methyl represented the most active alkyl substituent at the 2-position (cis) within this series.

To complete the SAR around the piperidine carboxylic acids, we combined the results of the 2- and 3-substitutions by preparing the cis dimethyl-substituted derivative. The two enantiomers were separated by chiral HPLC and showed very different activities (Table 3). The (–) enantiomer **31** was the most active compound prepared so far, while the (+) enantiomer **32** was somewhat less active than parental compound **2**.

Unfortunately, all attempts to obtain a cocrystal structure of **31** failed and we were thus not able to unambiguously determine the absolute stereochemistry. However, if it is assumed that the 3-substituent of **31** adopts the same stereochemistry as the ethyl group in the cocrystal structure of **23**, the absolute stereochemistry can be assigned as *R,R,R*.

In this absence of a cocrystal structure it is also difficult to judge whether the 4-fold improvement of **31** compared to **2** results from additional hydrophobic contacts or whether conformational locking also plays a role.

After optimization of the right side of the molecule to give a 4-fold improvement in potency by the addition of two methyl groups, it was decided to refocus on the left side of the molecule. Because of relative ease of synthesis, the unsubstituted piperidine acid was maintained for this purpose. Interestingly, the fragment-type compound **8** described above had shown the best ligand efficiency in this series so far. The introduction of the phenyl ring **7** leads to a more potent but less ligand efficient compound. It was envisaged that isosteric replacement of this group may lead to better ligand efficiency. The crystal structure of compound **5** in Nek2 shows a coplanar conformation between the phenyl and the pyrazine ring. It was decided to replace the phenyl ring with isosteric thiophene, since this should be able to engage in similar hydrophobic interaction as the phenyl ring and should relax steric interactions of the protons in this coplanar conformation. Indeed, thiophene **33** and in particular **34** showed good activity when compared to the unsubstituted phenyl compound **7** (Table 4).

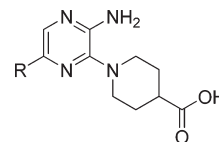
Additional hydrophobic substitutions on the thiophene were explored with the aim of improving activity without increasing TPSA. This was focused on the ortho position with respect to the pyrazine ring, since docking of compound **34** into Nek2 (data not shown) suggested that the other positions would point toward solvent.

Gratifyingly, substitution with an ethyl **35** or cyclopropyl **36** group led to an approximately 4-fold improvement in potency. Cyclopentyl compound **37** was slightly less active but still comparable to the unsubstituted thiophene derivative **34**.

We solved the cocrystal structure of compounds **35** and **36** with Nek2 (Figure 5). The ethyl group of **35** and the cyclopropyl group of **36** point toward the hinge region and occupy a hydrophobic pocket between Ile14 and Gly91–Gly92 similar to the methoxy group of compound **5**. This observation explains why groups larger than cyclopropyl in this position lead to loss of activity, since they cannot be accommodated in the same pocket because of steric repulsion.

Thiophene compounds **35** and **36** were submitted for PAMPA assay along with dimethylpiperidine **31**. All thiophenes showed improved permeation at pH 5 compared to hit compound **2** but still low permeation at physiological pH (Table 4).

Table 4. Replacement of the 3,4,5-Trimethoxyphenyl Ring of **2** by Thienyl Substituents^b



Compound	R	Nek2 IC ₅₀ (μM)	PAMPA pH 5 / 7.4 (10 ⁻⁶ cm/s)	LE ^a
7		7.8 (6.9, 8.6)	59.4 / 0.0	0.32
8	H	48.5	-	0.37
33		7.2	-	0.34
34		4.3	-	0.35
35		2.1 ± 1.0	>125 / 1.3	0.34
36		1.6 ± 0.7	>125 / 0.9	0.33
37		3.4	-	0.29

^a Ligand efficiency, calculated according to ref 21. ^b Results are the mean (±SD) for n ≥ 3 or the mean values of two independent determinations with individual determinations in parentheses or samples run at n = 1.

Unfortunately, the low permeation observed with all carboxylic acids described here at pH 7.4 correlated with a lack of effect in our cell based assay (IC₅₀ > 50 μM), which we recently described elsewhere²⁰ (data not shown), and we thus decided not to pursue this series further. However, we were intrigued by our observation of the Tyr-down conformation and decided to further investigate its significance for Nek2 inhibition. In this context, it is worth noting that we crystallized the unphosphorylated form of the kinase and that it is unlikely that the Tyr-down conformation would be adopted by the phosphorylated, fully active form. Unfortunately, all our attempts to crystallize the phosphorylated form of the kinase were unsuccessful. The activation loop will become more ordered (in a DFG-in conformation) upon phosphorylation, disfavoring the changes in the DFG motif associated with the Tyr-down conformation. Furthermore, this will bring the C helix and in particular a Leu residue (Leu59) closer to the gatekeeper, closing the hydrophobic pocket filled by Tyr70 in the Tyr-down conformation and forming the hydrophobic spine that is a feature of active kinase structures.³⁰ As a result, this part of the ATP pocket possibly adopts a

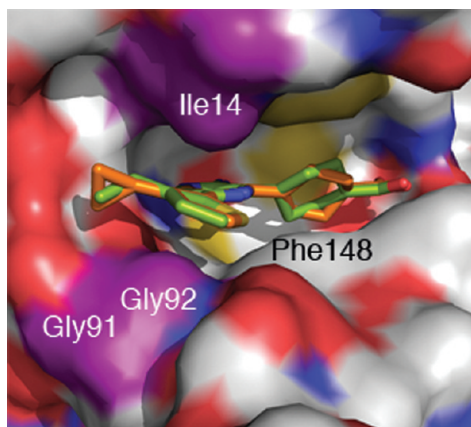


Figure 5. Ethyl group of compound **35** (C in green) and cyclopropyl group of compound **36** (C in orange) point toward the back of the catalytic pocket and are sandwiched between Ile14 of the Gly-rich loop and Gly91–Gly92 of the hinge region.

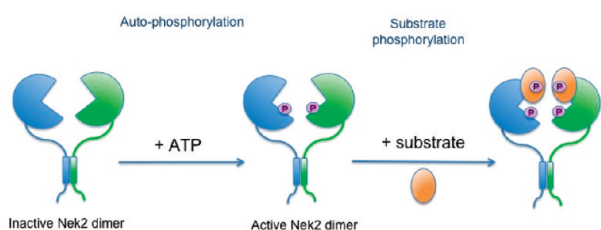


Figure 6. Autophosphorylation and substrate phosphorylation cascade. Addition of ATP to the inactive Nek2 dimer initiates trans-autophosphorylation on Thr175 and activation of the protein. This active form of Nek2 can then phosphorylate its substrate.

significantly different shape once the kinase has autophosphorylated.

However, inhibitors binding to the inactive Tyr-down conformation should be capable of inhibiting Nek2 autophosphorylation and activation. Inhibition of Nek2 autophosphorylation would be pharmaceutically desirable, since Nek2 is present in the unphosphorylated form during most of the cell cycle.

The kinase assay employed in this study so far was performed using the unphosphorylated kinase. Addition of ATP after preincubation with the compound initiates the cascade of trans-autophosphorylation on Thr175 and subsequent substrate phosphorylation (Figure 6).

This assay format therefore detects compounds that inhibit autophosphorylation and/or substrate phosphorylation. To further investigate the relevance of the Tyr-down conformation for Nek2 inhibition, a set of experiments was performed to test if a representative set of our compounds (**2**, **12**, **14**, **15**, **31**, and **35**) inhibit autophosphorylation or substrate phosphorylation or both. First, the kinase activity assay was performed by preincubation of the kinase with ATP to ensure complete phosphorylation of the enzyme before incubation with the inhibitor. This procedure only identifies inhibitors of substrate phosphorylation (step 2 in Figure 6). Second, a specific assay was developed to measure the autophosphorylation reaction using an antibody that recognizes the phosphorylated Thr175 of Nek2. Thus, this assay can only identify inhibitors of autophosphorylation (step 1 in Figure 6).

These results are shown in Table 5. All compounds inhibit autophosphorylation and substrate phosphorylation with comparable potencies. The significant inhibition of autophosphorylation suggests that the inactive Tyr-down conformation

Table 5. Potency of Selected Compounds against Nek2 Autophosphorylation and Substrate Phosphorylation^a

compd	Tyr70	IC ₅₀ (μM)	
		Nek2 autophosphorylation	Nek2 substrate phosphorylation
2	Tyr down	0.41 ± 0.14	0.94 (0.77, 1.1)
12	Tyr down	0.71 (0.56, 0.85)	1.6
14	Flexible	1.2 (1.0, 1.3)	2.3 (1.9, 2.7)
15	Tyr down	1.3 ± 0.3	2.5
31		0.3	0.2
35	Tyr down	0.72	1.9

^aResults are the mean (±SD) for $n \geq 3$ or the mean values of two independent determinations with individual determinations in parentheses or samples run at $n = 1$.

Table 6. Selectivity Data of Selected Compounds against Nek1, Plk1, and Chk1^a

compd	IC ₅₀ (μM)			
	Nek2	Nek1	Plk1	Chk1
2	0.87 ± 0.34	2.6 ± 1.1	22.6 ± 4.5	> 100
31	0.23 (0.19, 0.26)	0.17 (0.14, 0.19)	19.4 (15.1, 23.6)	> 100
35	2.1 ± 1.0	22.5 (15.6, 29.4)	8.5 (5.5, 11.4)	> 100

^aResults are the mean (±SD) for $n \geq 3$ or the mean values of two independent determinations with individual determinations in parentheses or samples run at $n = 1$.

observed in our cocrystal structure is indeed relevant for inhibitor design. The autophosphorylation data for compounds **14** and **15** are particularly noteworthy. Compound **14** inhibits autophosphorylation. However, as described above, in the cocrystal structure of **14** Tyr70 adopts more than one conformation. This observation indicates that potent inhibition of autophosphorylation does not require locking Tyr70 into the down conformation. Loss in enthalpy, e.g., caused by the breakage of interactions between the inhibitor and Tyr70, might be compensated by gain in entropy due to additional degrees of freedom of Tyr70.

As described above, **15** binds to the tyrosine down conformation, but the distance between the carboxylic acid group of **15** and the hydroxyl group of Tyr70 is too large (4 Å) for a hydrogen bond. The observation that this compound nevertheless shows activity in the autophosphorylation assay comparable to **12** and **14** indicates that other interactions, e.g., additional hydrophobic interactions between the methoxy group and the protein (Val68/Tyr70), compensate for the loss of the hydrogen bond.

These data emphasize the importance of structural data, since the observation that **12**, **14**, and **15** interact differently with Nek2 cannot be derived from biochemical data only.

Our data also suggested that compounds of this series can inhibit the kinase in both the phosphorylated and unphosphorylated states, which is ideal because it ensures that these inhibitors can bind to the enzyme and inhibit it during its entire lifespan, regardless of the phosphorylation stage.

To conclude our initial investigations, compounds **2**, **31**, and **35** were submitted for selectivity testing against Nek1, Plk1, and Chk1 (Table 6). Nek1 was chosen because it is the closest homologue to Nek2 and has several cellular functions, including ciliogenesis and DNA repair.^{31,32} Plk1 was chosen because it also features a Phe in the Phe148 equivalent position and because we wanted to avoid the effects associated with Plk1 inhibition. Chk1 was chosen because it is a cell cycle kinase without similarity to Nek2. The data are shown in Table 6. All compounds show good selectivity against Chk1,

which is not surprising given that Chk1 and Nek2 belong to different kinase families and are not closely related in terms of sequence.

A different picture emerged for Plk1 and Nek1. Hit compound **2** showed encouraging selectivity against Plk1, but thiophene **35** was less selective. The enhanced selectivity of compound **2** can be rationalized by the presence of the methoxy groups. The cocrystal structures of both compounds indicated that the methoxy groups are situated above Gly91 and Gly92. Plk1 features an Arg (Arg136) instead of Gly92 in Nek2, possibly leading to a steric clash with the methoxy group. The lack of selectivity of the thiophene derivative could therefore potentially be rectified by substitution off the thiophene toward Gly92. The improved activity of compound **31** translates into good selectivity (approximately 100-fold), again demonstrating that very good selectivity against Plk1 can be achieved in this series.

Finally all compounds show significant activity against Nek1, which is not surprising given that the sequences of Nek1 and Nek2 in the ATP pocket are identical except for an Ala to Cys switch (Cys22 in Nek2). However, compound **35** shows an approximately 10-fold selectivity against Nek1. In the absence of a Nek1 crystal structure this selectivity is difficult to rationalize.

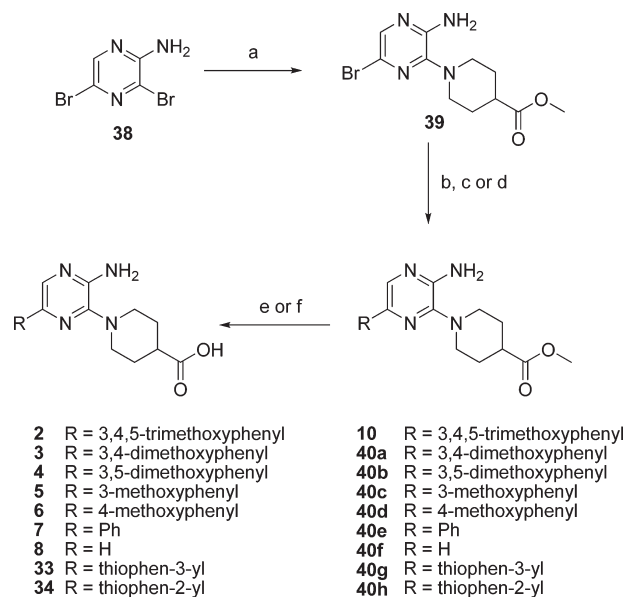
In conclusion, to the best of our knowledge, we have described the first systematic investigation of the structure–activity relationship of inhibitors of the mitotic kinase Nek2. We prepared several analogues of the aminopyrazine **2** by exploring structure-based design. Substitution on the piperidine ring led to compound **31** as the most active compound to date with good selectivity against Plk1. Replacement of the trimethoxyphenyl group of **2** by thiophene derivatives led to compounds with improved permeation.

The cocrystal structures presented here reveal that the pyrazine based inhibitor **2** and several of its analogues bind to an unusual inactive conformation of Nek2 referred to as the Tyr-down conformation. To our knowledge, the Tyr-down conformation has so far not been observed with any other class of kinase inhibitors. Our biochemical data confirm that these compounds inhibit autophosphorylation, as would be predicted for an inhibitor of the inactive kinase, supporting the hypothesis that this conformation can be explored for the design of autophosphorylation inhibitors.

A key feature of Nek2 is Phe148 which because of its central position in the ATP pocket and in concert with the large gatekeeper residue (Met86) profoundly affects inhibitor design. Very few other kinases possess this combination of a phenylalanine in this position and a large gatekeeper. One example is Plk1, and the cross-reactivity of compound **35** against Plk1 as well as the Nek2 activity in the recently published Plk1 inhibitors^{19,28} suggests that these kinases, which do not belong to the same kinase family, can be inhibited by similar chemotypes. We believe that this is at least partially due to the rare combination of this particular Phe and a large gatekeeper.

Interestingly, only very few potent Nek2 inhibitors have been published to date. We hypothesize that the strong geometric constraints introduced by the combination of Phe in this central position and the large Met gate keeper residue make Nek2 challenging to target, requiring an “exquisitely matched” inhibitor as observed for BI-2536 (**18**) in the case of Plk1.²⁸ We believe that our study presented here will aid the identification of more advanced inhibitors of Nek2 featuring such an exquisite match.

Scheme 1. Synthesis of Compounds **2–8**, **10**, **33**, and **34**^a



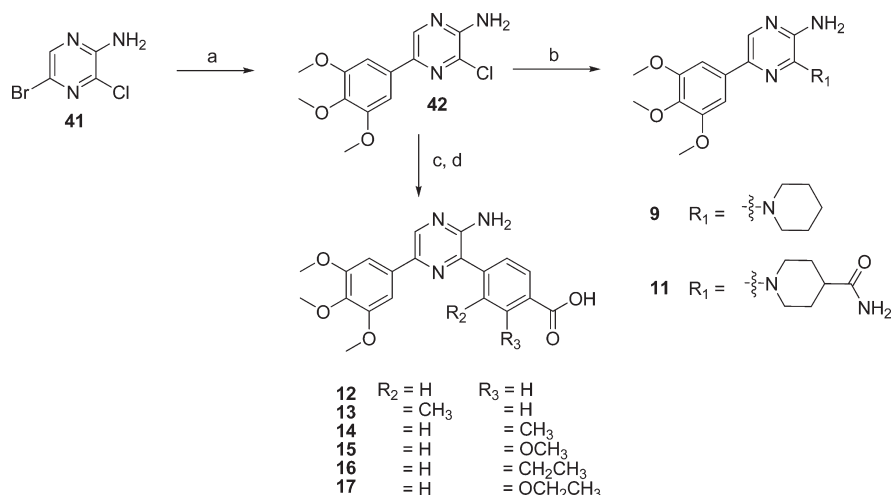
^a Reagents and conditions: (a) methyl piperidine-4-carboxylate, DIPEA, NMP, microwave, 140 °C. (b) For **10** and **40a–e**: ArB(OH)₂, Pd(PPh₃)₄, 2 M Na₂CO₃ (aq), DME, microwave, 100 °C. (c) For **40f**: H₂, 10% Pd/C, EtOH, room temp. (d) For **40g–h**: ArB(OH)₂, Pd(dppf)Cl₂·CH₂Cl₂, 2 M Na₂CO₃ (aq), DME, microwave, 105 °C. (e) For **2–8**: 1 M NaOH (aq), THF, room temp. (f) For **33–34**: 1 M NaOH (aq), MeOH, 65 °C.

Chemistry

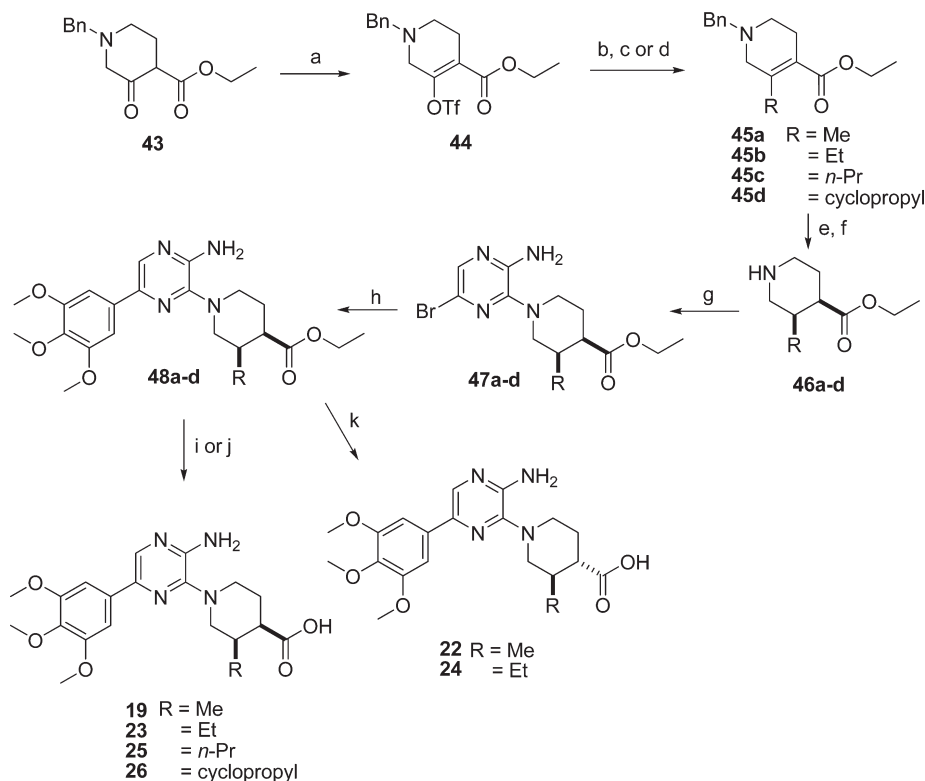
Compounds **2–8**, **10**, and **33–34** were prepared from common intermediate **39** (Scheme 1) which was formed by regioselective S_NAr reaction of methyl piperidine-4-carboxylate with commercially available 3,5-dibromopyrazin-2-amine (**38**). Reaction with the required phenylboronic acid under Suzuki conditions afforded the elaborated tricyclic core of the inhibitors. In the case of compound **40f**, dehalogenation was achieved by hydrogenation. Standard basic hydrolysis provided the final compounds in acceptable yields.

Modification of the right-hand side of the structure was achieved through use of common intermediate **42** (Scheme 2). This was constructed by chemoselective Suzuki coupling of 5-bromo-3-chloropyrazin-2-amine (**41**) with 3,4,5-trimethoxyphenylboronic acid. Subsequent S_NAr reaction with cyclic amines provided compounds **9** and **11**. Alternatively, compounds **12–17** were prepared by a second Suzuki coupling followed by base hydrolysis.

Synthesis of the 3-substituted piperidine compounds **19–26** is outlined in Scheme 3. Triflation of commercially available protected oxopiperidine **43** gave enol triflate **44**, which was used in either a Negishi³³ (**45a–c**) or Suzuki (**45d**) coupling to provide alkylated tetrahydropyridine intermediates. Debenzylation using ACE-Cl³⁴ and MeOH followed by hydrogenation using a platinum catalyst afforded the free amines **46a–d**. These were reacted with dihalopyrazine **41**, in a similar S_NAr procedure as previously described, to afford the desired products **47a–d** chemoselectively. Suzuki coupling with 3,4,5-trimethoxyphenylboronic acid and hydrolysis of the ester gave the cis 3-substituted piperidine compounds **19**, **23**, **25**, and **26**. Interestingly, hydrolysis of 3-cyclopropyl substituted compound **48d** under the usual basic conditions was unsuccessful and it was necessary to employ acidic conditions. Chiral HPLC resolution of ester **48a** followed by hydrolysis in the same manner afforded the enantiomerically pure

Scheme 2. Synthesis of Compounds 9 and 11–17^a

^a Reagents and conditions: (a) 3,4,5-trimethoxyphenylboronic acid, Pd(dppf)Cl₂·CH₂Cl₂, 2 M Na₂CO₃ (aq), DME, microwave, 80 °C; (b) R₂NH, DIPEA, NMP, microwave, 180 °C; (c) ArB(OR)₂, Pd(dppf)Cl₂·CH₂Cl₂, 2 M Na₂CO₃ (aq), DMF, microwave, 130 °C; (d) 1 M NaOH (aq), MeOH, 60 °C.

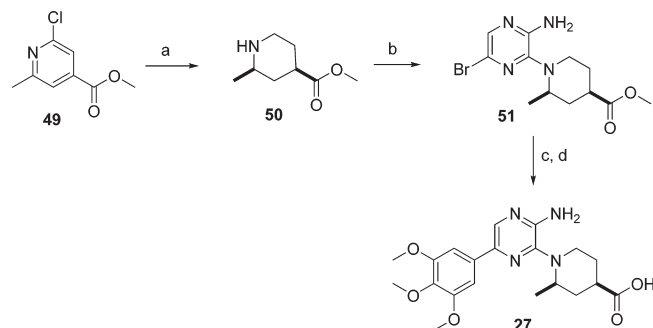
Scheme 3. Synthesis of Compounds 19–26^a

^a Reagents and conditions: (a) NaH, Et₂O, Tf₂O. (b) For **45a,b**: R₂Zn, Pd(PPh₃)₄, room temp. (c) For **45c**: *i*-Pr₂Zn, Pd(PPh₃)₄, room temp. (d) For **45d**: *c*-PrB(OH)₂, Pd(OAc)₂, PCy₃, K₃PO₄, toluene/water (9:1), microwave, 140 °C. (e) (i) ACE-Cl, DCE, reflux; (ii) MeOH, reflux; (f) H₂, 50 psi, PtO₂, AcOH, 50 °C; (g) **41**, DIPEA, NMP, microwave, 140 °C; (h) 3,4,5-trimethoxyphenylboronic acid, Pd(dppf)Cl₂·CH₂Cl₂, 2 M Na₂CO₃ (aq), DME, microwave, 100 °C. (i) For **19**, **23**, and **25**: 1 M NaOH (aq), MeOH, 60 °C. (j) For **26**: HCl, THF/H₂O (1:1), 70 °C; (k) (i) NaOEt, EtOH, reflux; (ii) 1 M NaOH (aq), MeOH, 60 °C.

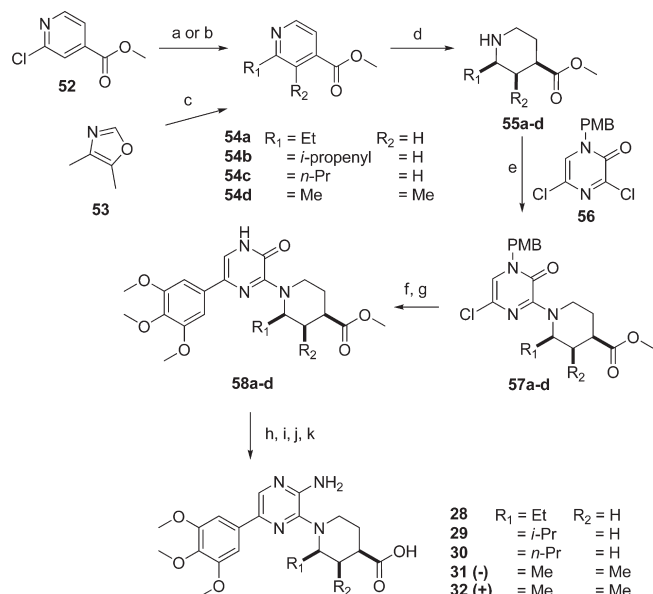
compounds **20** and **21**. Compounds **22** and **24** were formed by epimerization of the respective ester intermediates by prolonged heating with sodium ethoxide (to give the more energetically favored trans diastereoisomers)³⁵ followed by basic hydrolysis.

2-Methyl substituted piperidine compound **27** was prepared in four steps beginning with hydrogenation of methyl 2-chloro-6-methylisonicotinate (**49**) (Scheme 4). The resulting piperidine **50** reacted very poorly under standard S_NAr conditions,

possibly because of the increased steric bulk around the nucleophilic center. However, use of dibromopyridine **38**, in place of 3-chloro-5-bromopyridine **41**, along with silver oxide and prolonged heating at 180 °C provided adequate product (as the hydrolyzed ester), albeit in 6% yield, to complete the synthesis of **27** after re-esterification, Suzuki coupling, and base hydrolysis. The regioselectivity of the S_NAr reaction was confirmed in the final product by observation of a NOE

Scheme 4. Synthesis of Compound 27^a

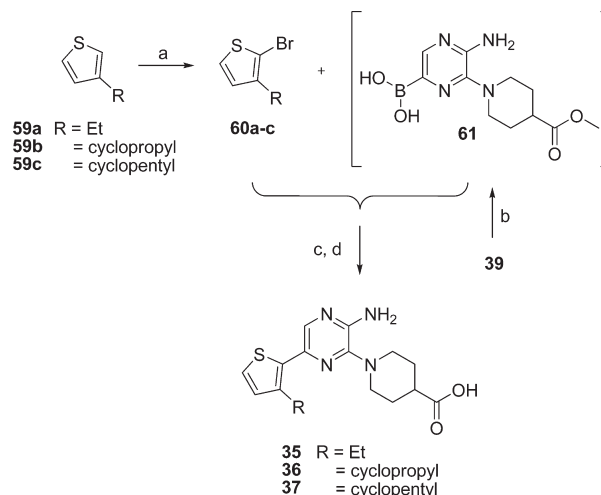
^a Reagents and conditions: (a) H₂, H-Cube, 10% Pt/C, AcOH, 70 °C; (b) **38**, Ag₂O, DIPEA, NMP, microwave, 180 °C; (c) 3,4,5-trimethoxyphenylboronic acid, Pd(dppf)Cl₂·CH₂Cl₂, 2 M Na₂CO₃ (aq), DME, microwave, 100 °C; (d) 1 M NaOH (aq), MeOH, 60 °C.

Scheme 5. Synthesis of Compounds 28–32^a

^a Reagents and conditions. (a) For **54a** and **54c**: RMgBr, Fe(acac)₃, THF/NMP (9:1), room temp. (b) For **54b**: (i) isopropenylboronic acid pinacol ester, Pd(OAc)₂, SPhos, K₃PO₄, MeCN/H₂O (3:2), microwave, 130 °C; (ii) MeOH, HCl, reflux. (c) For **54d**: methyl acrylate, hydroquinone, benzene, reflux. (d) H₂, 50 psi, PtO₂, 50 °C; (e) DIPEA, NMP, microwave, 140 °C; (f) (3,4,5-trimethoxyphenyl)tributyltin, Pd₂(dba)₃, SPhos, CsF, MeCN, microwave, 160 °C; (g) CF₃SO₂OH, TFA/CH₂Cl₂ (1:1), room temp; (h) Tf₂O, DIPEA, CHCl₃, room temp; (i) PMB-NH₂, Pd(OAc)₂, BINAP, K₃PO₄, MeCN, microwave, 110 °C; (j) CF₃SO₂OH, TFA/DCM (1:1), room temp; (k) 1 M NaOH (aq), MeOH, 60 °C.

between the protons at the 2/6-position of the trimethoxyphenyl group and the pyrazine proton.

The synthesis of alternative 2-alkyl substituted piperidines **28–32** was achieved by either iron(III) catalyzed alkylation³⁶ (**54a** and **54c**) or Suzuki coupling (**54b**) of chloropyridine **52** followed by hydrogenation with a platinum catalyst (Scheme 5). 2,3-Dimethylpiperidine **55d** was synthesized by hydrogenation of dimethylpyridine **54d** which was formed by reaction of dimethylloxazole **53** with methyl acrylate.³⁷ Given the difficulty encountered in S_NAr reaction of 2-methylpiperidine **50** with halopyrazines, an alternative route to compounds **28–32** was devised involving regioselective S_NAr reaction with the more reactive PMB-protected dichloropyrazinone **56**.^{38,39} Installation of the trimethoxyphenyl group was achieved

Scheme 6. Synthesis of Compounds 35–37^a

^a Reagents and conditions: (a) NBS, AcOH, CHCl₃, room temp; (b) bis(pinacolato)diboron, Pd(dppf)Cl₂·CH₂Cl₂, KOAc, DMF, microwave, 105 °C; (c) Pd(dppf)Cl₂·CH₂Cl₂, 2 M Na₂CO₃ (aq), DME, microwave, 105 °C; (d) 1 M NaOH (aq), MeOH, 65 °C.

through Stille coupling,⁴⁰ as this does not require a base like the corresponding Suzuki reaction which led to decomposition of the starting material. PMB deprotection did not occur with TFA at reflux, but the use of 3.5 equiv of trifluoromethylsulfonic acid (TfOH) promoted the reaction at room temperature to furnish the tricyclic core. Unfortunately, treatment of the pyrazinone with iodoacetamide^{41,42} did not convert it directly to the aminopyrazine, as planned, necessitating a more protracted route involving triflation, Buchwald coupling with PMB-amine, and deprotection using TfOH. Finally, basic hydrolysis afforded the desired compounds **28–30**. Compounds **31** and **32** were prepared by hydrolysis of the corresponding enantiomerically pure esters which were obtained from chiral HPLC separation.

The alkylthiophene compounds **35–37** were synthesized by Suzuki coupling of the appropriate 3-alkyl-2-bromothiophene with pyrazineboronic acid **61** followed by hydrolysis of the ester (Scheme 6). The 3-alkyl-2-bromothiophenes were made by regioselective bromination⁴³ at the 2-position of commercially available 3-ethylthiophene (**59a**), 3-cyclopropylthiophene (synthesized by Suzuki coupling of cyclopropylboronic acid with 3-bromothiophene),⁴⁴ or 3-cyclopentylthiophene.⁴⁵ The pyrazinylboronic acid coupling partner was made from bromopyrazine **39** using palladium catalysis and was used crude.

Experimental Section

Nek2 Caliper Methodology. Kinase activity was measured in a microfluidic assay that monitors the separation of a phosphorylated product from its substrate. The assay was run on a Caliper EZ Reader II (Caliper Life Sciences Ltd., Runcorn, U.K.) using separation buffer (no. 760367 Caliper LS) containing CR-8 (500 nM, no. 760278, Caliper LS). In 384-well polypropylene plates (no. 781280, Greiner Bio-One, Gloucestershire, U.K.), compound stocks (10 mM) were diluted 1:4 in 100% DMSO and then sequentially diluted 1:3 in DMSO to make an eight-point dilution curve (2500–1.1 μM). The compounds were further diluted 1:20 into kinase buffer (50 mM HEPES, 0.02% NaN₃, 0.01% BSA, 0.1 mM sodium orthovanadate, 1 mM DTT, 5 mM MgCl₂, 0.1% Tween 20) before 4 μL was transferred into a 384-well polypropylene assay plate, equivalent to a final concentration range of 50–0.02 μM in 2% DMSO.

To this assay plate, Nek2 (2 μL , 4 nM final, no. PV3360 Invitrogen), peptide 11 (5-FAM-KKLNRTLVA-COOH, 2 μL , 1 μM final, no. 760355 Caliper LS), and ATP (2 μL , 30 μM final) all diluted in kinase buffer were added. The plate was sealed and centrifuged (1 min, 1000 rpm) before incubation for 1 h at room temperature. The reaction was stopped by the addition of separation buffer (90 μL). The plate was read on an EZ Reader II (Caliper LS) using a 12-sipper chip (760137-0372R, Caliper LS) using instrument settings of pressure -1.8 psi and voltage 1850 ΔV . The percentage conversion of product from substrate was generated automatically by the instrument, and the percentage inhibition was calculated relative to blank wells (containing no enzyme and 2% DMSO) and total wells (containing all reagents and 2% DMSO). IC_{50} values were calculated in GraphPad Prism 5 using a nonlinear regression fit of the log (inhibitor) versus response with variable slope equation.

Nek2 Autophosphorylation Assay. Autophosphorylation activity was measured in a DELFIA assay that monitors autophosphorylation of Nek2 using a specific phospho-Nek2 antibody. This antibody was raised to the T175 autophosphorylation site of Nek2 by immunizing rabbits with a CSFAKT(P)FVGTPE peptide (synthesised by J Metcalfe, ICR) conjugated to KLH and affinity purified prior to use (Open Biosystems, Huntsville, AL, USA). In 384-well polypropylene plates (no. 781280, Greiner Bio-One, Gloucestershire, U.K.), compound stocks (10 mM) were diluted 1:4 in 100% DMSO and then sequentially diluted 1:3 in DMSO to make an eight-point dilution curve (2500–1.1 μM). The compounds were further diluted 1:20 into kinase buffer (50 mM HEPES, 0.02% NaN_3 , 0.01% BSA, 0.1 mM sodium orthovanadate, 1 mM DTT, 5 mM MgCl_2) before 20 μL was transferred into a 384-well polypropylene assay plate equivalent to a final concentration range of 50–0.02 μM in 2% DMSO. To this assay plate, Nek2 (10 μL , 4 nM final, no. PV3360 Invitrogen) was added. The plate was then briefly shaken and incubated for 5 min at room temperature. The reaction was started with the addition of ATP (20 μL , 30 μM final). After 50 s of incubation time the reaction was stopped by the addition of stop buffer (50 μL , 50 mM HEPES, 0.02% NaN_3 , 0.01% BSA, 0.1 mM sodium orthovanadate, 1 mM DTT, and 10 mM EDTA). The reaction mixture (50 μL) was transferred to an Immulon 2 high bind plate (no. 3455, Thermo Scientific, Loughborough, Leicestershire, U.K.) and left to coat overnight at 4 $^\circ\text{C}$. The plates were washed four times with wash buffer (0.1% Tween 20, WellWash4, Thermo Life Sciences) before being blocked with 5% milk in PBS (100 μL) for 30 min at 37 $^\circ\text{C}$. The plate was washed a further two times with wash buffer before the addition of primary phospho-T175 antibody (50 μL). The plate was incubated for 2 h at 37 $^\circ\text{C}$. The plate was washed a further four times with wash buffer before the addition of europium labeled secondary antibody (50 μL , no. AD0105, anti-rabbit IgG, 0.25 $\mu\text{g}/\text{mL}$ final, PerkinElmer Life Sciences, Seer Green, Buckinghamshire, U.K.) diluted in DELFIA assay buffer (no. 4002-0010, PerkinElmer Life Sciences). The plates were washed a further four times with wash buffer before the addition of enhancement solution (no. 4001-0010, 50 $\mu\text{L}/\text{well}$, PerkinElmer Life Sciences). The plate was read on an Envision 2103 multilabel counter (PerkinElmer Life Sciences) using a time-resolved measurement mode reading fluorescence at 615 nm. The percentage inhibition was calculated relative to blank wells (containing no enzyme and 2% DMSO) and total wells (containing all reagents and 2% DMSO). IC_{50} values were calculated in GraphPad Prism 5 using a nonlinear regression fit of the log (inhibitor) versus response with variable slope equation.

Plk1 Caliper Methodology. In 384-well polypropylene plates (Greiner Bio-One, Gloucestershire, U.K.), compound stocks (10 mM) were diluted 1:2 in 100% DMSO and then sequentially diluted 1:3 in DMSO to make an eight-point dilution curve (5000–2.3 μM). The compounds were further diluted 1:20 into kinase buffer (50 mM MOPS, pH 6.5, 0.004% Triton-X-100, 1 mM DTT, 5 mM MgCl_2) before 4 μL was transferred into a 384-well polypropylene assay plate equivalent to a final concentration

range of 100–0.046 μM in 2% DMSO. To this assay plate, Plk1 (2 μL , 18 nM final, 05-157, Carma Biosciences-Kinase Logistics ApS, Denmark), peptide (5-FAM-RRRAGALMDASFEQ-CONH₂, 2 μL , 2 μM final, Pepceuticals, Nottingham, U.K.), and ATP (2 μL , 15 μM final) all diluted in kinase buffer were added. The plate was sealed and centrifuged (1 min, 1000 rpm) before incubation for 75 min at room temperature. The reaction was stopped by the addition of separation buffer (70 μL). The plate was read in the same manner as for Nek2.

Nek1 Caliper Methodology. In 384-well polypropylene plates (Greiner Bio-One, Gloucestershire, U.K.), compound stocks (10 mM) were diluted 1:2 in 100% DMSO and then sequentially diluted 1:3 in DMSO to make an eight-point dilution curve (5000–2.3 μM). The compounds were further diluted 1:20 into kinase buffer (50 mM HEPES, 0.02% NaN_3 , 0.01% BSA, 0.1 mM sodium orthovanadate, 1 mM DTT, 5 mM MgCl_2 , 0.1% Tween 20) before 4 μL was transferred into a 384-well polypropylene assay plate equivalent to a final concentration range of 100–0.046 μM in 2% DMSO. To this assay plate, Nek1 (2 μL , 4 nM final, PV4202 Invitrogen), peptide 11 (5-FAM-KKLNRTLVA-COOH, 2 μL , 1 μM final, no. 760355 Caliper LS), and ATP (2 μL , 60 μM final) all diluted in kinase buffer were added. The plate was sealed and centrifuged (1 min, 1000 rpm) before incubation for 1 h at room temperature. The reaction was stopped by the addition of separation buffer (90 μL). The plate was read in the same manner as for Nek2.

TPSA. Molecular polar surface area was calculated using Pipeline Pilot, version 7, incorporating nitrogen, oxygen, phosphorus, and sulfur as described.⁴⁶

Cocrystallization of Nek2 with Ligands. Structures were experimentally determined as previously described.²³

General Chemistry Information. Starting materials, reagents, and solvents for reactions were reagent grade and used as purchased. Microwave experiments were conducted using a CEM Discover synthesis unit. The machine provides a continuous focused microwave delivery system. The power output can be varied from 0 to 300 W. Reactions were performed in glass vessels (~10 mL) sealed with a septum. The pressure was monitored by a gauge needle through the septum, and the temperature was monitored by an infrared probe at the bottom of the glass vessel. Chromatography solvents were HPLC grade and were used without further purification. Thin layer chromatography (TLC) analysis was performed using Merck silica gel 60 F-254 thin layer plates. Flash column chromatography was carried out using columns prepacked with 40–63 μm silica. NMR spectra were recorded on a Bruker Advance 500 MHz spectrometer, and samples were referenced to the appropriate internal nondeuterated solvent peak. In the case where a 1:1 mixture of MeOD and CDCl_3 was used, the samples were referenced to MeOD. The data are given as follows: chemical shift (δ) in ppm, multiplicity (where applicable), coupling constants (J) in Hz (where applicable), and integration (where applicable). LC-MS analyses were performed on a Micromass LCT/Waters Alliance 2795 separations module HPLC system with a Merck Chromolith SpeedROD RP-18e 50 mm \times 4.6 mm column at a temperature of 22 $^\circ\text{C}$. The following solvent system, at a flow rate of 2 mL/min, was used: solvent A, methanol; solvent B, 0.1% formic acid in water. Gradient elution was as follows: 1:9 (A/B) to 9:1 (A/B) over 2.25 min, 9:1 (A/B) for 0.75 min and then reversion back to 1:9 (A/B) over 0.3 min, 1:9 (A/B) for 0.2 min. Detection was with a Waters 2487 dual λ absorbance detector (detecting at 254 nm), and ionization was electrospray (ESI). Some LC-MS and all HRMS analyses were performed on a Agilent 1200 series HPLC system with a Merck Chromolith SpeedROD RP-18e 50 mm \times 4.6 mm column at a temperature of 22 $^\circ\text{C}$. The following solvent system, at a flow rate of 2 mL/min, was used: solvent A, methanol; solvent B, 0.1% formic acid in water. Gradient elution was as follows: 1:9 (A/B) to 9:1 (A/B) over 2.5 min, 9:1 (A/B) for 1 min and then reversion back to 1:9 (A/B) over 0.3 min, 1:9 (A/B) for 0.2 min. This was connected to

a Agilent 6200 time of flight (ToF) mass spectrometer (simultaneous ESI and APCI or ESI only) with detection at 254 nm. The following reference masses were used for HRMS analysis: caffeine $[M + H]^+ = 195.087652$, reserpine $[M + H]^+ = 609.280657$, and (1*H*,1*H*,3*H*-tetrafluoropentoxy)phosphazene $[M + H]^+ = 922.009798$. The purity of final compounds was determined by HPLC as described above and are $\geq 95\%$ unless specified otherwise.

Ethyl 1-benzyl-5-(trifluoromethylsulfonyloxy)-1,2,3,6-tetrahydropyridine-4-carboxylate (44). Sodium hydride 60% (0.37 g, 9.36 mmol) was washed under N_2 with dry hexane (5 mL). Ether (5 mL) was added, and the suspension was cooled to 0 °C. Ethyl 1-benzyl-3-oxo-4-piperidinecarboxylate (1.22 g, 4.68 mmol) in ether (23 mL) was then added, and the resulting slurry was stirred at ambient temperature for 1 h. After the mixture was recooled to 0 °C, trifluoromethanesulfonic anhydride (1.19 mL, 7.02 mmol) was added dropwise. The mixture was stirred for 30 min and then warmed to ambient temperature and stirred for 1.5 h before being cooled to 0 °C and water (75 mL) was added dropwise. The mixture was extracted with CH_2Cl_2 (3×75 mL), and the combined organic layers were dried over $MgSO_4$, concentrated, and dried in vacuo. The crude material was purified by flash column chromatography (0–30% EtOAc in hexane) to give triflate **44** (1.82 g, 99%) as a pale orange oil: 1H NMR (500 MHz, $CDCl_3$) δ 7.50–7.14 (m, 4H), 4.29 (q, $J = 7.2$ Hz, 1H), 3.64 (s, 2H), 3.18 (t, $J = 2.6$ Hz, 1H), 2.65 (t, $J = 8.5$ Hz, 1H), 2.61–2.55 (m, 1H), 1.32 (t, $J = 7.2$ Hz, 2H); ^{13}C NMR (126 MHz, $CDCl_3$) δ 163.7, 148.8, 137.0, 128.8, 128.5, 127.6, 121.4, 118.3 (q, $J = 319.9$ Hz), 61.7, 61.2, 53.2, 48.2, 26.0, 14.0; LC-MS m/z 394 $[M + H]^+$; HRMS (ESI) m/z calcd for $C_{16}H_{19}F_3NO_5S$ $[M + H]^+ 394.09305$, found 394.09307.

General Procedure A: Ethyl 1-benzyl-5-methyl-1,2,3,6-tetrahydropyridine-4-carboxylate (45a). To a stirred solution of triflate **44** (1.13 g, 2.88 mmol) and tetrakis(triphenylphosphine)palladium(0) (0.33 g, 0.29 mmol) in THF (72 mL) at 0 °C was added dimethylzinc (1 M in toluene, 4.9 mL, 4.9 mmol). The mixture was allowed to warm to ambient temperature and stirred for 24 h. Water (100 mL) and brine (100 mL) were added, and the mixture was extracted with EtOAc (2×100 mL) and CH_2Cl_2 (2×50 mL). The organic layers were combined, dried over $MgSO_4$, and concentrated in vacuo. The crude material was purified by flash column chromatography (0–45% EtOAc in hexane) to give *N*-benzylmethyltetrahydropyridine **45a** (0.67 g, 90%): 1H NMR (500 MHz, $CDCl_3$) δ 7.37–7.29 (m, 4H), 7.29–7.23 (m, 1H), 4.18 (q, $J = 7.1$ Hz, 2H), 3.58 (s, 2H), 2.99 (t, $J = 1.9$ Hz, 2H), 2.55 (t, $J = 5.8$ Hz, 2H), 2.50–2.31 (m, 2H), 1.98 (s, 3H), 1.27 (t, $J = 7.1$ Hz, 3H); ^{13}C NMR (126 MHz, $CDCl_3$) δ 167.7, 144.7, 137.9, 129.0, 128.2, 127.1, 122.4, 62.2, 59.8, 59.3, 49.4, 26.8, 19.2, 14.3; LC-MS m/z 260 $[M + H]^+$; HRMS (ESI) m/z calcd for $C_{16}H_{22}NO_2$ $[M + H]^+ 260.16451$, found 260.16527.

Compound **45b** was synthesized in a similar manner, and the data are available in the Supporting Information.

General Procedure B: Ethyl 5-methyl-1,2,3,6-tetrahydropyridine-4-carboxylate. To a stirred solution of *N*-benzylmethyltetrahydropyridine **45a** in dichloroethane (40 mL) under N_2 at 0 °C was added dropwise α -chloroethyl chloroformate (0.29 mL, 2.71 mmol). The mixture was then heated at reflux for 1 h. The solvent was concentrated in situ, and dry MeOH (20 mL) was added. This mixture was heated at reflux for 2 h and then concentrated in vacuo. This material was partitioned between CH_2Cl_2 (50 mL) and 1 M aqueous NaOH (50 mL). The aqueous layer was separated and extracted with CH_2Cl_2 (2×50 mL). The organic layers were combined, dried over $MgSO_4$, concentrated in vacuo, and used crude in the next step.

General Procedure C: (\pm)-(3*R*,4*R*)-Ethyl 3-methylpiperidine-4-carboxylate (46a). The crude debenzylated product (0.53 g, 2.58 mmol) was dissolved in AcOH (50 mL), and platinum dioxide (0.06 g, 0.26 mmol) was added. The mixture was hydrogenated in a Parr apparatus at 50 psi and 40 °C for 21 h. It was then filtered through Celite and washed with EtOAc. The filtrate was evaporated and then partitioned between 1 M aqueous

KOH (50 mL) and CH_2Cl_2 /MeOH (9:1, 50 mL). The aqueous layer was extracted with CH_2Cl_2 /MeOH (9:1, 2×50 mL). The combined organic extracts were combined, dried over $MgSO_4$, and concentrated in vacuo. The crude material was purified by flash column chromatography (0–10%, 1 M methanolic ammonia in CH_2Cl_2) to give 3-methylpiperidine **46a** as a clear oil which became a white crystalline solid on standing (0.30 g, 68% (two steps)): 1H NMR (500 MHz, $CDCl_3$) δ 4.15–4.02 (m, 2H), 3.05 (dt, $J = 12.4, 4.0$ Hz, 1H), 2.84 (dd, $J = 12.5, 4.0$ Hz, 1H), 2.78 (dd, $J = 12.5, 3.5$ Hz, 1H), 2.60 (ddd, $J = 12.4, 10.1, 4.0$ Hz, 1H), 2.55 (dt, $J = 10.1, 4.0$ Hz, 1H), 2.41 (br s, 1H), 2.09 (m, 1H), 1.76 (dtd, $J = 14.0, 10.1, 4.0$ Hz, 1H), 1.61 (dq, $J = 14.0, 4.0$ Hz, 1H), 1.21 (t, $J = 7.1$ Hz, 3H), 0.92 (d, $J = 7.1$ Hz, 3H); ^{13}C NMR (126 MHz, $CDCl_3$) δ 174.2, 60.0, 51.5, 44.8, 44.4, 31.0, 24.3, 14.2, 13.6; LC-MS m/z 172 $[M + H]^+$; HRMS (ESI) m/z calcd for $C_9H_{17}NO_2$ $[M + H]^+ 172.13321$, found 172.13339.

Compounds **46b–d** were synthesized in a similar manner, and the data are available in the Supporting Information.

General Procedure D: (\pm)-(3*R*,4*R*)-Ethyl 1-(3-amino-6-bromopyrazin-2-yl)-3-methylpiperidine-4-carboxylate (47a). 2-Amino-5-bromo-3-chloropyrazine (**41**) (0.44 g, 2.109 mmol), 3-methylpiperidine **46a** (0.301 g, 1.76 mmol), and DIPEA (0.46 mL, 2.64 mmol) were dissolved in NMP (4.4 mL) in a microwave vial under N_2 . The mixture was then heated at 140 °C for 1 h 20 min in a microwave. Then 1 M KOH (50 mL) was added and the mixture was extracted with CH_2Cl_2 (3×50 mL). The organic layers were combined, dried over $MgSO_4$, and separated from NMP using a Biotage SCX-2 column (5 g) and eluting with 0–10% MeOH in CH_2Cl_2 and then 50% methanolic ammonia in CH_2Cl_2 . The crude material was purified by flash column chromatography (0–30% EtOAc in hexane) to give bromopyrazinyl-3-methylpiperidine **47a** (0.42 g, 70%): 1H NMR (500 MHz, $CDCl_3$) δ 7.70 (s, 1H), 4.64 (br s, 2H), 4.25–4.03 (m, 2H), 3.49 (dtd, $J = 12.5, 4.1, 1.7$ Hz, 1H), 3.39 (ddd, $J = 12.5, 3.9, 1.7$ Hz, 1H), 2.91 (dd, $J = 12.5, 3.1$ Hz, 1H), 2.82 (ddd, $J = 12.5, 11.2, 3.1$ Hz, 1H), 2.62 (dt, $J = 11.0, 4.4$ Hz, 1H), 2.42–2.35 (m, 1H), 2.01 (dtd, $J = 17.9, 11.2, 4.1$ Hz, 1H), 1.89–1.80 (m, 1H), 1.26 (t, $J = 7.1$ Hz, 3H), 1.07 (d, $J = 7.0$ Hz, 3H); ^{13}C NMR (126 MHz, $CDCl_3$) δ 173.7, 147.2, 146.9, 136.6, 124.3, 60.3, 53.8, 47.7, 44.2, 30.9, 23.0, 14.2, 13.6; LC-MS m/z 343, 345 $[M + H]^+$; HRMS (ESI) m/z calcd for $C_{13}H_{20}^{79}BrN_4O_2$ $[M + H]^+ 343.07641$, found 343.07696.

Compounds **47b–d** were synthesized in a similar manner, and the data are available in the Supporting Information.

General Procedure E: (\pm)-(3*R*,4*R*)-Ethyl 1-(3-amino-6-(3,4,5-trimethoxyphenyl)pyrazin-2-yl)-3-methylpiperidine-4-carboxylate (48a). Bromopyrazinyl-3-methylpiperidine **47a** (0.09 g, 0.25 mmol), trimethoxyphenylboronic acid (0.08 g, 0.38 mmol), Pd(dppf)- $Cl_2 \cdot CH_2Cl_2$ (0.02 g, 0.03 mmol), and aqueous Na_2CO_3 solution (2 M, 0.25 mL, 0.50 mmol) were dissolved in DME (0.5 mL) in a microwave vial under argon and heated in a microwave at 105 °C for 2 h. Water (10 mL) was added, and the mixture was extracted with CH_2Cl_2 (3×10 mL). The organic layers were combined, dried over $MgSO_4$, and concentrated in vacuo. The crude material was purified by flash column chromatography (0–80% EtOAc in hexane) to give trimethoxyphenylpyrazine **48a** (0.10 g, 96%): 1H NMR (500 MHz, $CDCl_3$) δ 8.08 (s, 1H), 7.13 (s, 2H), 4.70 (br s, 2H), 4.23–4.14 (m, 2H), 3.93 (s, 6H), 3.87 (s, 3H), 3.63–3.57 (m, 1H), 3.48 (ddd, $J = 12.4, 3.8, 1.3$ Hz, 1H), 3.01 (dd, $J = 12.5, 3.0$ Hz, 1H), 2.94 (td, $J = 12.5, 2.9$ Hz, 1H), 2.67 (dt, $J = 11.0, 4.4$ Hz, 1H), 2.50–2.39 (m, 1H), 2.17–2.03 (m, 1H), 1.95–1.86 (m, 1H), 1.28 (t, $J = 7.1$ Hz, 3H), 1.13 (d, $J = 7.0$ Hz, 3H); ^{13}C NMR (126 MHz, $CDCl_3$) δ 174.0, 153.5, 147.2, 146.4, 140.3, 138.3, 133.2, 132.0, 103.0, 60.9, 60.3, 56.2, 54.1, 47.8, 44.5, 31.1, 23.3, 14.3, 13.8; LC-MS m/z 431 $[M + H]^+$; HRMS (ESI) m/z calcd for $C_{22}H_{31}N_4O_5$ $[M + H]^+ 431.2289$, found 431.2288.

Compounds **48b–d** were synthesized in a similar manner, and the data are available in the Supporting Information.

(+)-(3*S*,4*S*)-Ethyl 1-(3-amino-6-(3,4,5-trimethoxyphenyl)pyrazin-2-yl)-3-methylpiperidine-4-carboxylate. The enantiomers were separated by semipreparative chiral HPLC (Chiralpak IA column (250 mm × 10 mm), detection at $\lambda = 254$ nm, isocratic elution 100% IPA, flow rate of 2.0 mL/min, run time of 60 min) $t_{(+)} = 27.5$ min; analytical HPLC (IA Chiralpak column, detection $\lambda = 254$ nm, injection volume of 5 μ L, isocratic elution 100% IPA, flow rate of 0.25 mL/min, run time of 65 min) $t_{(+)} = 42.5$ min, 97% ee; $[\alpha]_D^{20} + 10$ (c 0.35, MeOH).

(-)-(3*R*,4*R*)-Ethyl 1-(3-amino-6-(3,4,5-trimethoxyphenyl)pyrazin-2-yl)-3-methylpiperidine-4-carboxylate. Continued semipreparative chiral HPLC (as above) $t_{(-)} = 32.7$ min; analytical HPLC (as above) $t_{(-)} = 49.5$ min, 93% ee; $[\alpha]_D^{20} - 10$ (c 0.36, MeOH).

General Procedure F: (\pm)-(3*R*,4*R*)-1-(3-Amino-6-(3,4,5-trimethoxyphenyl)pyrazin-2-yl)-3-methylpiperidine-4-carboxylic Acid (**19**). ((Trimethoxyphenyl)pyrazinyl)methylpiperidine ester **48a** (19 mg, 0.044 mmol) was dissolved in methanol (3.7 mL), and aqueous NaOH solution (1 M, 3.7 mmol, 3.7 mL) was added. The mixture was then heated at 60 °C for 2 h. After cooling to ambient temperature, the solution was made pH 5 by careful addition of aqueous 1 M HCl (and aqueous 1 M NaOH if necessary) which, upon standing, produced a precipitate. This was filtered, washed with a cold mixture of water/MeOH (3:2), and dried in vacuo to give methylpiperidine carboxylic acid **19** (8 mg, 45%): $^1\text{H NMR}$ (500 MHz, CDCl_3) δ 8.00 (s, 1H), 7.12 (s, 2H), 5.34 (br s, 2H), 3.94 (s, 6H), 3.88 (s, 3H), 3.66–3.60 (m, 1H), 3.52 (dd, $J = 12.5, 2.9$ Hz, 1H), 3.04 (dd, $J = 12.5, 2.9$ Hz, 1H), 3.02–2.96 (m, 1H), 2.76 (dt, $J = 10.9, 4.3$ Hz, 1H), 2.55–2.48 (m, 1H), 2.17–2.07 (m, 1H), 1.99–1.92 (m, 1H), 1.22 (d, $J = 6.8$ Hz, 3H); $^{13}\text{C NMR}$ (126 MHz, CDCl_3) δ 178.3, 153.6, 147.0, 147.0, 140.1, 138.5, 132.8, 129.9, 103.0, 60.9, 56.3, 54.1, 47.8, 44.3, 31.1, 23.2, 13.8; LC-MS m/z 403 $[\text{M} + \text{H}]^+$; HRMS (ESI) m/z calcd for $\text{C}_{20}\text{H}_{27}\text{N}_4\text{O}_5$ $[\text{M} + \text{H}]^+$ 403.19760, found 403.19750.

Compounds **23** and **25** were synthesized in a similar manner, and the data are available in the Supporting Information.

General Procedure G: (-)-(3*S*,4*S*)-1-(3-Amino-6-(3,4,5-trimethoxyphenyl)pyrazin-2-yl)-3-methylpiperidine-4-carboxylic Acid (**20**). Preparation was from (+)-((trimethoxyphenyl)pyrazinyl)methylpiperidine ester (4 mg, 0.010 mmol) according to general procedure F but with the following workup procedure: the solution was made pH 5 by careful addition of aqueous 1 M HCl (and aqueous 1 M NaOH if necessary) and was extracted with $\text{CH}_2\text{Cl}_2/\text{MeOH}$ (9:1, 3 × 5 mL). The combined organic layers were dried over MgSO_4 , concentrated, and dried in vacuo to give (-)-ethylpiperidine carboxylic acid **20** (4 mg, 99%, purity 94%): $[\alpha]_D^{20} - 24$ (c 0.36, MeOH); LC-MS m/z 403 $[\text{M} + \text{H}]^+$; HRMS (ESI) m/z calcd for $\text{C}_{20}\text{H}_{27}\text{N}_4\text{O}_5$ $[\text{M} + \text{H}]^+$ 403.1976, found 403.1983.

(+)-(3*R*,4*R*)-1-(3-Amino-6-(3,4,5-trimethoxyphenyl)pyrazin-2-yl)-3-methylpiperidine-4-carboxylic Acid (**21**). Preparation from (-)-((trimethoxyphenyl)pyrazinyl)methylpiperidine ester (4 mg, 0.010 mmol) according to general procedure G gave (+)-ethylpiperidine carboxylic acid (4 mg, 99%): $[\alpha]_D^{20} + 33$ (c 0.36, MeOH); LC-MS m/z 403 $[\text{M} + \text{H}]^+$; HRMS (ESI) m/z calcd for $\text{C}_{20}\text{H}_{27}\text{N}_4\text{O}_5$ $[\text{M} + \text{H}]^+$ 403.1976, found 403.1990.

Methyl 2,3-dimethylisonicotinate (54d). 4,5-Dimethylloxazole³⁷ (**53**) (3.12 g, 32.1 mmol), methyl acrylate (5.8 mL, 64.3 mmol), and hydroquinone (0.03 g, 0.28 mmol) were dissolved in benzene (6.2 mL) and heated at reflux for 18 h. The solvent was concentrated in vacuo, and the crude material was purified by flash column chromatography (0–50% EtOAc in hexane) to give methyl 2,3-dimethylisonicotinate (**54d**) (2.36 g, 44%): $^1\text{H NMR}$ (500 MHz, CDCl_3) δ 8.39 (d, $J = 5.1$ Hz, 1H), 7.39 (d, $J = 5.1$ Hz, 1H), 3.91 (s, 3H), 2.58 (s, 3H), 2.45 (s, 3H); $^{13}\text{C NMR}$ (126 MHz, CDCl_3) δ 167.5, 159.1, 146.2, 137.9, 130.8, 120.7, 52.4, 23.3, 15.9; LC-MS m/z 166 $[\text{M} + \text{H}]^+$; HRMS (ESI) m/z calcd for $\text{C}_9\text{H}_{12}\text{NO}_2$ $[\text{M} + \text{H}]^+$ 166.0863, found 166.0868.

General Procedure H: (\pm)-(2*R*,3*R*,4*R*)-Methyl 2,3-dimethylpiperidine-4-carboxylate (**55d**). To a solution of dimethylisoni-

cotinate **54d** (0.59 g, 3.57 mmol) in acetic acid (40 mL) was added PtO_2 (0.07 g, 0.29 mmol). The mixture was then hydrogenated in a Parr apparatus at 50 bar and 50 °C for 18 h. It was then filtered through Celite and concentrated in vacuo. Aqueous 1 M NaOH (50 mL) was added, and the mixture was extracted with $\text{CH}_2\text{Cl}_2/\text{MeOH}$ (9:1, 3 × 50 mL). The organic layers were combined, dried over MgSO_4 , and concentrated in vacuo. The crude material was purified by flash column chromatography (0–10%, 1 M methanolic ammonia in CH_2Cl_2) to give dimethylpiperidine **55d** (0.47 g, 77%): $^1\text{H NMR}$ (500 MHz, CDCl_3) δ 3.68 (s, 3H), 3.15 (ddd, $J = 12.7, 4.4, 2.1$ Hz, 1H), 2.88 (qd, $J = 6.6, 2.9$ Hz, 1H), 2.65 (td, $J = 12.7, 3.2$ Hz, 1H), 2.57 (dt, $J = 12.7, 4.0$ Hz, 1H), 2.52 (s, 1H), 2.16–2.09 (m, 1H), 1.77 (qd, $J = 12.7, 4.4$ Hz, 1H), 1.67–1.60 (m, 1H), 1.08 (d, $J = 6.6$ Hz, 1H), 0.83 (d, $J = 7.0$ Hz, 3H); $^{13}\text{C NMR}$ (126 MHz, CDCl_3) δ 174.6, 55.0, 51.2, 46.7, 46.1, 34.9, 21.9, 19.7, 6.8; LC-MS m/z 172 $[\text{M} + \text{H}]^+$; HRMS (ESI) m/z calcd for $\text{C}_9\text{H}_{18}\text{NO}_2$ $[\text{M} + \text{H}]^+$ 172.13321, found 172.13299.

Compounds **54a–c** were synthesized in a similar manner, and the data are available in the Supporting Information.

General Procedure I: (\pm)-(2*R*,3*R*,4*R*)-Methyl 1-(6-chloro-4-(4-methoxybenzyl)-3-oxo-3,4-dihydropyrazin-2-yl)-2,3-dimethylpiperidine-4-carboxylate (**57d**). 3,5-Dichloro-1-(4-methoxybenzyl)pyrazin-2(1*H*)-one (**56**) (0.47 g, 2.73 mmol) was dissolved in NMP (6.5 mL). DIPEA (0.54 mL, 3.12 mmol) and 2,3-dimethylpiperidine **55d** (0.47 g, 2.73 mmol) were added, and the mixture was heated in a microwave at 140 °C for 2 h. The DIPEA was then removed by concentration in vacuo, and the crude material, including NMP solvent, was purified by flash column chromatography (0–20% EtOAc in hexane) to give dimethylpiperidinylpyrazinone **57d** (0.60 g, 55%): $^1\text{H NMR}$ (500 MHz, CDCl_3) δ 7.25–7.21 (m, 2H), 6.89–6.85 (m, 2H), 6.57 (s, 1H), 4.95–4.89 (m, 1H), 4.92 (d, $J = 14.1$ Hz, 1H), 4.85 (d, $J = 14.1$ Hz, 1H), 4.59 (dt, $J = 13.8, 3.3$ Hz, 1H), 3.78 (s, 3H), 3.69 (s, 3H), 3.53 (ddd, $J = 14.0, 12.5, 3.3$ Hz, 1H), 2.64 (td, $J = 5.5, 3.3$ Hz, 1H), 2.29–2.21 (m, 1H), 2.08 (dq, $J = 13.8, 3.3$ Hz, 1H), 1.88–1.78 (m, 1H), 1.15 (d, $J = 7.0$ Hz, 3H), 1.11 (d, $J = 7.4$ Hz, 3H); $^{13}\text{C NMR}$ (126 MHz, CDCl_3) δ 175.4, 159.6, 151.3, 150.8, 129.8, 127.3, 125.7, 114.3, 114.0, 55.2, 53.3, 51.5, 51.2, 41.0, 37.9, 36.3, 27.2, 16.6, 11.8; LC-MS m/z 420 $[\text{M} + \text{H}]^+$; HRMS (ESI) m/z calcd for $\text{C}_{21}\text{H}_{27}\text{ClN}_3\text{O}_4$ $[\text{M} + \text{H}]^+$ 420.16846, found 420.16963.

Compounds **57a–c** were synthesized in a similar manner, and the data are available in the Supporting Information.

General Procedure J: (\pm)-(2*R*,3*R*,4*R*)-Methyl 1-(4-(4-methoxybenzyl)-3-oxo-6-(3,4,5-trimethoxyphenyl)-3,4-dihydropyrazin-2-yl)-2,3-dimethylpiperidine-4-carboxylate. Dimethylpiperidinylpyrazinone **57d** (0.54 g, 1.29 mmol), (3,4,5-trimethoxyphenyl)-tributyltin⁴⁰ (1.18 g, 2.57 mmol), cesium fluoride (0.65 g, 4.24 mmol), $\text{Pd}_2(\text{dba})_3$ (18 mg, 19 μ mol), SPhos (32 mg, 0.077 mmol), and acetonitrile (19 mL) were combined and heated in a microwave at 160 °C for 80 min. CH_2Cl_2 (20 mL) was added, and the mixture was filtered. The filtrate was concentrated in vacuo and purified by flash column chromatography (0–20% EtOAc in hexane) to give trimethoxyphenylpyrazinone (0.48 g, 68%): $^1\text{H NMR}$ (500 MHz, CDCl_3) δ 7.30–7.26 (m, 2H), 7.01 (s, 1H), 6.94 (s, 2H), 6.88–6.84 (m, 2H), 5.08 (d, $J = 14.3$ Hz, 1H), 4.99 (d, $J = 14.3$ Hz, 1H), 4.89–4.83 (m, 1H), 4.54–4.47 (m, 1H), 3.88 (s, 6H), 3.84 (s, 3H), 3.77 (s, 3H), 3.70 (s, 3H), 3.66–3.59 (m, 1H), 2.69–2.64 (m, 1H), 2.39–2.31 (m, 1H), 2.11 (dq, $J = 13.6, 3.2$ Hz, 1H), 1.90 (ddt, $J = 13.6, 11.9, 4.9$ Hz, 1H), 1.22 (d, $J = 7.0$ Hz, 1H), 1.13 (d, $J = 7.4$ Hz, 1H); $^{13}\text{C NMR}$ (126 MHz, CDCl_3) δ 175.5, 159.4, 153.3, 151.6, 151.5, 137.9, 132.6, 130.8, 129.4, 127.8, 114.5, 114.2, 102.4, 60.8, 56.1, 55.2, 53.5, 51.8, 51.2, 41.5, 38.5, 36.2, 27.0, 16.4, 11.9; LC-MS m/z 552 $[\text{M} + \text{H}]^+$; HRMS (ESI) m/z calcd for $\text{C}_{30}\text{H}_{38}\text{N}_3\text{O}_7$ $[\text{M} + \text{H}]^+$ 552.27043, found 552.27210.

General Procedure K: (\pm)-(2*R*,3*R*,4*R*)-Methyl 2,3-dimethyl-1-(3-oxo-6-(3,4,5-trimethoxyphenyl)-3,4-dihydropyrazin-2-yl)-piperidine-4-carboxylate (**58d**). Trimethoxyphenylpyrazinone (0.48 g, 0.87 mmol) was dissolved in a mixture of trifluoroacetic acid and CH_2Cl_2 (1:1, 33 mL). Trifluoromethanesulfonic acid (0.27 mL, 3.05 mmol) was then added and the mixture

stirred at ambient temperature for 17 h. It was then concentrated, and saturated NaHCO₃ solution (50 mL) was added. The mixture was extracted with CH₂Cl₂ (3 × 50 mL), and the organic layers were combined, dried over MgSO₄, and concentrated in vacuo. The crude material was purified by flash column chromatography (0–70% EtOAc in CH₂Cl₂) to give deprotected pyrazinone **58d** (0.21 g, 57%): ¹H NMR (500 MHz, CDCl₃) δ 12.09 (s, 1H), 7.14 (s, 1H), 7.03 (s, 2H), 4.87–4.79 (m, 1H), 4.53 (dt, *J* = 13.6, 3.5 Hz, 1H), 3.91 (s, 6H), 3.87 (s, 3H), 3.72 (s, 3H), 3.71–3.63 (m, 1H), 2.72–2.66 (m, 1H), 2.43–2.35 (m, 1H), 2.14 (dq, *J* = 13.5, 3.5 Hz, 1H), 1.96–1.84 (m, 1H), 1.24 (d, *J* = 7.0 Hz, 3H), 1.16 (d, *J* = 7.3 Hz, 3H); ¹³C NMR (126 MHz, CDCl₃) δ 175.4, 153.3 (2C), 151.2, 137.7, 132.4, 132.1, 111.4, 102.2, 60.8, 56.0, 53.2, 51.2, 41.5, 38.5, 36.0, 26.9, 16.3, 11.9; LC–MS *m/z* 432 [M + H]⁺; HRMS (ESI) *m/z* calcd for C₂₂H₃₀N₃O₆ [M + H]⁺ 432.212 91, found 432.213 10.

Compounds **58a–c** were synthesized in a similar manner, and the data are available in the Supporting Information.

General Procedure L: (±)-(2R,3R,4R)-Methyl 2,3-dimethyl-1-(3-(trifluoromethylsulfonyloxy)-6-(3,4,5-trimethoxyphenyl)pyrazin-2-yl)piperidine-4-carboxylate. Deprotected pyrazinone **58d** (0.10 g, 0.23 mmol) was dissolved in CHCl₃ (7.5 mL) and cooled to 0 °C. DIPEA (0.06 mL, 0.36 mmol) was added followed by trifluoromethanesulfonic anhydride (0.06 mL, 0.36 mmol). The mixture was warmed to ambient temperature and stirred for 1 h. The solvent was then removed by concentration in vacuo and the crude material was purified by flash column chromatography (0–40% EtOAc in hexane) to give pyrazine triflate (0.10 g, 82%): ¹H NMR (500 MHz, CDCl₃) δ 8.21 (s, 1H), 7.20 (s, 2H), 3.94 (s, 6H), 3.90 (s, 3H), 3.90–3.85 (m, 1H), 3.72 (s, 3H), 3.58 (ddd, *J* = 12.6, 6.6, 3.8 Hz, 1H), 3.22 (ddd, *J* = 12.6, 8.7, 3.6 Hz, 1H), 2.69 (dt, *J* = 8.8, 4.5 Hz, 1H), 2.41–2.30 (m, 1H), 2.24–2.14 (m, 1H), 1.91–1.80 (m, 1H), 1.19 (d, *J* = 6.6 Hz, 3H), 1.08 (d, *J* = 7.1 Hz, 3H); ¹³C NMR (126 MHz, CDCl₃) δ 174.7, 153.7, 150.4, 149.7, 144.1, 140.2, 130.6, 130.1, 118.4 (q, *J* = 320.6 Hz), 104.4, 60.9, 56.2, 56.0, 51.5, 47.1, 44.2, 36.4, 24.0, 15.1, 11.9; LC–MS *m/z* 564 [M + H]⁺; HRMS (ESI) *m/z* calcd for C₂₃H₂₉F₃N₃O₈S [M + H]⁺ 564.162 20, found 564.163 42.

General Procedure M: (±)-(2R,3R,4R)-Methyl 1-(3-(4-methoxybenzylamino)-6-(3,4,5-trimethoxyphenyl)pyrazin-2-yl)-2,3-dimethylpiperidine-4-carboxylate. Pyrazine triflate (0.04 g, 0.06 mmol), 4-methoxybenzylamine (0.02 mL, 0.16 mmol), and potassium phosphate (0.02 g, 0.08 mmol) were dissolved in MeCN (1.6 mL). Palladium(II) acetate (1.6 mg, 7 μmol) and BINAP (7 mg, 0.012 mmol) were added. Then the mixture was heated in a microwave at 110 °C for 1 h. CH₂Cl₂ (10 mL) was added, and the mixture was filtered through cotton wool and concentrated in vacuo. The crude material was purified by flash column chromatography (0–30% EtOAc in hexane) to give 4-methoxybenzylaminopyrazine (0.02 g, 43%): ¹H NMR (500 MHz, CDCl₃) δ 8.24 (s, 1H), 7.29–7.24 (m, 2H), 7.10 (s, 2H), 6.91–6.86 (m, 2H), 5.87 (s, 1H), 4.63 (dd, *J* = 14.4, 5.3 Hz, 1H), 4.59 (dd, *J* = 14.4, 5.4 Hz, 1H), 3.93 (s, 6H), 3.87 (s, 3H), 3.81 (s, 3H), 3.71 (s, 3H), 3.48 (qd, *J* = 6.3, 2.8 Hz, 1H), 3.15–3.06 (m, 1H), 2.78–2.67 (m, 2H), 2.34–2.25 (m, 1H), 1.99 (qd, *J* = 13.0, 4.3 Hz, 1H), 1.80 (dd, *J* = 13.8, 2.8 Hz, 1H), 0.95 (d, *J* = 6.3 Hz, 3H), 0.92 (d, *J* = 6.9 Hz, 3H); ¹³C NMR (126 MHz, CDCl₃) δ 174.5, 158.9, 153.6, 149.9, 145.7, 138.4, 138.1, 134.5, 133.3, 131.3, 128.5, 114.1, 102.7, 100.0, 60.9, 57.9, 56.2, 55.3, 51.8, 51.6, 46.5, 44.6, 36.3, 22.6, 17.7, 8.5; LC–MS *m/z* 551 [M + H]⁺; HRMS (ESI) *m/z* calcd for C₃₀H₃₉N₄O₆ [M + H]⁺ 551.286 41, found 551.286 84.

General Procedure N: (±)-(2R,3R,4R)-Methyl 1-(3-amino-6-(3,4,5-trimethoxyphenyl)pyrazin-2-yl)-2,3-dimethylpiperidine-4-carboxylate. 4-Methoxybenzylaminopyrazine (18 mg, 0.033 mmol) was dissolved in a mixture of trifluoroacetic acid and CH₂Cl₂ (1:1, 3 mL), and trifluoromethanesulfonic acid (10 μL, 0.13 mmol) was added. The mixture was stirred at ambient temperature for 2 h. It was then concentrated, and saturated NaHCO₃ solution (5 mL) was added. The mixture was extracted

with CH₂Cl₂ (3 × 5 mL), the organic layers were combined, dried over MgSO₄, and concentrated in vacuo. The crude material was purified by flash column chromatography (0–50% EtOAc in CH₂Cl₂) to give aminopyrazinylpiperidine ester (13 mg, 92%): ¹H NMR (500 MHz, CDCl₃) δ 8.16 (s, 1H), 7.10 (s, 2H), 5.10 (s, 2H), 3.94 (s, 6H), 3.88 (s, 3H), 3.73 (s, 3H), 3.51 (qd, *J* = 6.2, 2.8 Hz, 1H), 3.23–3.16 (m, 1H), 2.77–2.64 (m, 2H), 2.36–2.28 (m, 1H), 2.05 (qd, *J* = 13.0, 4.3 Hz, 1H), 1.87–1.78 (m, 1H), 1.00 (d, *J* = 2.5 Hz, 3H), 0.98 (d, *J* = 3.1 Hz, 3H); ¹³C NMR (126 MHz, CDCl₃) δ 174.6, 153.6, 150.1, 145.7, 140.5, 138.4, 133.9, 132.9, 102.9, 60.9, 57.7, 56.2, 51.6, 51.5, 46.5, 36.3, 22.6, 17.7, 8.6; LC–MS *m/z* 431 [M + H]⁺; HRMS (ESI) *m/z* calcd for C₂₂H₃₁N₄O₅ [M + H]⁺ 431.228 90, found 431.230 09.

(–)-(2R,3R,4R)-Methyl 1-(3-amino-6-(3,4,5-trimethoxyphenyl)pyrazin-2-yl)-2,3-dimethylpiperidine-4-carboxylate. The enantiomers were separated by semipreparative chiral HPLC (Chiralpak IA column (250 mm × 10 mm), detection at λ = 254 nm, isocratic elution 5% IPA in MeCN, flow rate of 1.2 mL/min, run time of 30 min) *t*_(–) = 15.0 min; analytical HPLC (IA Chiralpak column, detection λ = 254 nm, injection volume of 5 μL, isocratic elution 5% IPA in MeCN, flow rate of 0.25 mL/min, run time of 30 min) *t*_(–) = 20.8 min, 98% ee; [α]_D²⁰ –65 (c 0.36, MeOH).

(+)-(2S,3S,4S)-Methyl 1-(3-amino-6-(3,4,5-trimethoxyphenyl)pyrazin-2-yl)-2,3-dimethylpiperidine-4-carboxylate. Continued semipreparative chiral HPLC (as above) *t*₍₊₎ = 16.7 min; analytical HPLC (as above) *t*₍₊₎ = 23.2 min, 87% ee; [α]_D²⁰ +35 (c 0.36, MeOH).

(–)-(2R,3R,4R)-1-(3-Amino-6-(3,4,5-trimethoxyphenyl)pyrazin-2-yl)-2,3-dimethylpiperidine-4-carboxylic Acid (31). Preparation from (–)-aminopyrazine ester (13 mg, 0.030 mmol) according to general procedure F gave (–)-dimethylpiperidine carboxylic acid **31** (9 mg, 72%): [α]_D²⁰ –57 (c 0.34, MeOH). LC–MS *m/z* 417 [M + H]⁺; HRMS (ESI) *m/z* calcd for C₂₁H₂₉N₄O₅ [M + H]⁺ 417.213 25, found 417.211 80. NMR characterization of the racemate: ¹H NMR (500 MHz, CDCl₃) δ 8.09 (s, 1H), 7.10 (d, *J* = 5.1 Hz, 2H), 5.73 (br s, 2H), 3.95 (s, 6H), 3.89 (s, 3H), 3.55 (qd, *J* = 6.3, 2.8 Hz, 1H), 3.28–3.20 (m, 1H), 2.80 (dt, *J* = 12.5, 3.9 Hz, 1H), 2.73 (td, *J* = 12.2, 2.5 Hz, 1H), 2.44–2.37 (m, 1H), 2.12–2.01 (m, 1H), 1.92–1.84 (m, 1H), 1.09 (d, *J* = 6.9 Hz, 3H), 1.03 (d, *J* = 6.3 Hz, 3H); ¹³C NMR (126 MHz, CDCl₃) δ 178.8, 153.7, 150.0, 146.5, 140.1, 138.5, 132.5, 131.9, 102.9, 60.9, 57.9, 56.3, 51.5, 46.5, 36.3, 22.5, 17.7, 8.6.

(+)-(2S,3S,4S)-1-(3-Amino-6-(3,4,5-trimethoxyphenyl)pyrazin-2-yl)-2,3-dimethylpiperidine-4-carboxylic Acid (32). Preparation from (+)-aminopyrazine ester (11 mg, 0.026 mmol) according to general procedure F gave (+)-dimethylpiperidine carboxylic acid **32** (7 mg, 66%): [α]_D²⁰ +56 (c 0.34, MeOH); LC–MS *m/z* 417 [M + H]⁺; HRMS (ESI) *m/z* calcd for C₂₁H₂₉N₄O₅ [M + H]⁺ 417.213 25, found 417.213 38.

Acknowledgment. We acknowledge NHS funding to the NIHR Biomedical Research Centre and funding from Cancer Research UK Programme Grant No. C309/A8274. R.B. acknowledges support from Cancer Research UK (Grant C24461/A10285 and infrastructure support for Structural Biology at the ICR), a Royal Society Research Fellowship, and the Career Development Programme of the ICR. We are thankful to Prof. Julian Blagg, Prof. Roger Griffin, and Prof. Paul Workman for helpful discussions. We also thank Dr. Amin Mirza, Meirion Richards, and Dr. Maggie Liu for their help with HPLC, NMR, and mass spectrometry and Yasmin Asad and Dr. Florence Raynaud for performing the PAMPA assay. We are indebted to the staff of DIAMOND (beamlines I02, I03, and I04) and ESRF (beamlines ID14, ID23, and ID29) as well as our many colleagues of the Section of Structural Biology (ICR in London) for their support during data collection. We acknowledge the reviewers for helpful comments.

Supporting Information Available: Experimental protocols and analytical data for final compounds **2–17**, **23–30**, **33–37** and all intermediates, summary of crystallographic analysis of compounds **2**, **12**, **14**, **15**, **17**, **23**, **35**, and **36** (Table S1), and description of PAMPA assay. This material is available free of charge via the Internet at <http://pubs.acs.org>.

References

- O'Regan, L.; Blot, J.; Fry, A. M. Mitotic regulation by NIMA-related kinases. *Cell Div.* **2007**, *2*, 25.
- Fry, A. M.; Meraldi, P.; Nigg, E. A. A centrosomal function for the human Nek2 protein kinase, a member of the NIMA family of cell cycle regulators. *EMBO J.* **1998**, *17*, 470–481.
- Fry, A. M.; Mayor, T.; Meraldi, P.; Stierhof, Y. D.; Tanaka, K.; Nigg, E. A. C-Nap1, a novel centrosomal coiled-coil protein and candidate substrate of the cell cycle-regulated protein kinase Nek2. *J. Cell Biol.* **1998**, *141*, 1563–1574.
- Bahe, S.; Stierhof, Y. D.; Wilkinson, C. J.; Leiss, F.; Nigg, E. A. Rootletin forms centriole-associated filaments and functions in centrosome cohesion. *J. Cell Biol.* **2005**, *171*, 27–33.
- Rapley, J.; Baxter, J. E.; Blot, J.; Wattam, S. L.; Casenghi, M.; Meraldi, P.; Nigg, E. A.; Fry, A. M. Coordinate regulation of the mother centriole component Nlp by Nek2 and Plk1 protein kinases. *Mol. Cell Biol.* **2005**, *25*, 1309–1324.
- Di Agostino, S.; Fedele, M.; Chieffì, P.; Fusco, A.; Rossi, P.; Geremia, R.; Sette, C. Phosphorylation of high-mobility group protein A2 by Nek2 kinase during the first meiotic division in mouse spermatocytes. *Mol. Biol. Cell* **2004**, *15*, 1224–1232.
- Chen, Y.; Riley, D. J.; Zheng, L.; Chen, P. L.; Lee, W. H. Phosphorylation of the mitotic regulator protein Hecl by Nek2 kinase is essential for faithful chromosome segregation. *J. Biol. Chem.* **2002**, *277*, 49408–49416.
- Fry, A. M.; Schultz, S. J.; Bartek, J.; Nigg, E. A. Substrate specificity and cell cycle regulation of the Nek2 protein kinase, a potential human homolog of the mitotic regulator NIMA of *Aspergillus nidulans*. *J. Biol. Chem.* **1995**, *270*, 12899–12905.
- Hames, R. S.; Wattam, S. L.; Yamano, H.; Bacchieri, R.; Fry, A. M. APC/C-mediated destruction of the centrosomal kinase Nek2A occurs in early mitosis and depends upon a cyclin A-type D-box. *EMBO J.* **2001**, *20*, 7117–7127.
- Eto, M.; Elliott, E.; Prickett, T. D.; Brautigan, D. L. Inhibitor-2 regulates protein phosphatase-1 complexed with NIMA-related kinase to induce centrosome separation. *J. Biol. Chem.* **2002**, *277*, 44013–44020.
- Hayward, D. G.; Fry, A. M. Nek2 kinase in chromosome instability and cancer. *Cancer Lett.* **2006**, *237*, 155–166.
- Faragher, A. J.; Fry, A. M. Nek2A kinase stimulates centrosome disjunction and is required for formation of bipolar mitotic spindles. *Mol. Biol. Cell* **2003**, *14*, 2876–2889.
- Hayward, D. G.; Clarke, R. B.; Faragher, A. J.; Pillai, M. R.; Hagan, I. M.; Fry, A. M. The centrosomal kinase Nek2 displays elevated levels of protein expression in human breast cancer. *Cancer Res.* **2004**, *64*, 7370–7376.
- Fletcher, L.; Cerniglia, G. J.; Nigg, E. A.; Yend, T. J.; Muschel, R. J. Inhibition of centrosome separation after DNA damage: a role for Nek2. *Radiat. Res.* **2004**, *162*, 128–135.
- Kokuryo, T.; Senga, T.; Yokoyama, Y.; Nagino, M.; Nimura, Y.; Hamaguchi, M. Nek2 as an effective target for inhibition of tumorigenic growth and peritoneal dissemination of cholangiocarcinoma. *Cancer Res.* **2007**, *67*, 9637–9642.
- Tsunoda, N.; Kokuryo, T.; Oda, K.; Senga, T.; Yokoyama, Y.; Nagino, M.; Nimura, Y.; Hamaguchi, M. Nek2 as a novel molecular target for the treatment of breast carcinoma. *Cancer Sci.* **2009**, *100*, 111–116.
- Suzuki, K.; Kokuryo, T.; Senga, T.; Yokoyama, Y.; Nagino, M.; Hamaguchi, M. Novel combination treatment for colorectal cancer using Nek2 siRNA and cisplatin. *Cancer Sci.* **2010**, *101*, 1163–1169.
- Qiu, X. L.; Li, G.; Wu, G.; Zhu, J.; Zhou, L.; Chen, P. L.; Chamberlin, A. R.; Lee, W. H. Synthesis and biological evaluation of a series of novel inhibitor of Nek2/Hecl analogues. *J. Med. Chem.* **2009**, *52*, 1757–1767.
- Emmitte, K. A.; Adjabeng, G. M.; Andrews, C. W.; Alberti, J. G.; Bambal, R.; Chamberlain, S. D.; Davis-Ward, R. G.; Dickson, H. D.; Hassler, D. F.; Hornberger, K. R.; Jackson, J. R.; Kuntz, K. W.; Lansing, T. J.; Mook, R. A., Jr.; Nailor, K. E.; Pobanz, M. A.; Smith, S. C.; Sung, C. M.; Cheung, M. Design of potent thiophene inhibitors of polo-like kinase 1 with improved solubility and reduced protein binding. *Bioorg. Med. Chem. Lett.* **2009**, *19*, 1694–1697.
- Hayward, D. G.; Newbatt, Y.; Pickard, L.; Byrne, E.; Mao, G.; Burns, S.; Sahota, N. K.; Workman, P.; Collins, I.; Aherne, W.; Fry, A. M. Identification by high-throughput screening of viridin analogs as biochemical and cell-based inhibitors of the cell cycle-regulated Nek2 kinase. *J. Biomol. Screening* **2010**, *15*, 918–927.
- Hopkins, A. L.; Groom, C. R.; Alex, A. Ligand efficiency: a useful metric for lead selection. *Drug Discovery Today* **2004**, *9*, 430–431.
- Martin, Y. C. A bioavailability score. *J. Med. Chem.* **2005**, *48*, 3164–3170.
- Richards, M. W.; O'Regan, L.; Mas-Droux, C.; Blot, J. M.; Cheung, J.; Hoelder, S.; Fry, A. M.; Bayliss, R. An autoinhibitory tyrosine motif in the cell-cycle-regulated Nek7 kinase is released through binding of Nek9. *Mol. Cell* **2009**, *36*, 560–570.
- Hilton, S.; Naud, S.; Caldwell, J. J.; Boxall, K.; Burns, S.; Anderson, V. E.; Antoni, L.; Allen, C. E.; Pearl, L. H.; Oliver, A. W.; Wynne Aherne, G.; Garrett, M. D.; Collins, I. Identification and characterisation of 2-aminopyridine inhibitors of checkpoint kinase 2. *Bioorg. Med. Chem.* **2010**, *18*, 707–718.
- Zuccotto, F.; Ardini, E.; Casale, E.; Angiolini, M. Through the "gatekeeper door": Exploiting the active kinase conformation. *J. Med. Chem.* **2010**, *53*, 2681–2694.
- Westwood, I.; Cheary, D. M.; Baxter, J. E.; Richards, M. W.; van Montfort, R. L.; Fry, A. M.; Bayliss, R. Insights into the conformational variability and regulation of human Nek2 kinase. *J. Mol. Biol.* **2009**, *386*, 476–485.
- The sequence alignment containing 491 human ePK kinase domains, available at <http://www.kinase.com>, was used to identify the occurrence and frequency of amino acids at specific positions within the catalytic domain.
- Kothe, M.; Kohls, D.; Low, S.; Coli, R.; Rennie, G. R.; Feru, F.; Kuhn, C.; Ding, Y. H. Selectivity-determining residues in Plk1. *Chem. Biol. Drug Des.* **2007**, *70*, 540–546.
- Kothe, M.; Kohls, D.; Low, S.; Coli, R.; Cheng, A. C.; Jacques, S. L.; Johnson, T. L.; Lewis, C.; Loh, C.; Nonomiya, J.; Sheils, A. L.; Verdries, K. A.; Wynn, T. A.; Kuhn, C.; Ding, Y. H. Structure of the catalytic domain of human polo-like kinase 1. *Biochemistry* **2007**, *46*, 5960–5971.
- Kornev, A. P.; Haste, N. M.; Taylor, S. S.; Eyck, L. F. Surface comparison of active and inactive protein kinases identifies a conserved activation mechanism. *Proc. Natl. Acad. Sci. U.S.A.* **2006**, *103*, 17783–17788.
- Quarmby, L. M.; Mahjoub, M. R. Caught Nek-ing: cilia and centrioles. *J. Cell Sci.* **2005**, *118*, 5161–5169.
- Polci, R.; Peng, A.; Chen, P. L.; Riley, D. J.; Chen, Y. NIMA-related protein kinase 1 is involved early in the ionizing radiation-induced DNA damage response. *Cancer Res.* **2004**, *64*, 8800–8803.
- Marshall, J. A.; Van Devender, E. A. Synthesis of (–)-deoxypukalide, the enantiomer of a degradation product of the furanocembranolide pukalide. *J. Org. Chem.* **2001**, *66*, 8037–8041.
- Olofson, R. A.; Martz, J. T.; Senet, J.-P.; Piteau, M.; Malfroot, T. A new reagent for the selective, high-yield N-dealkylation of tertiary amines: improved syntheses of naltrexone and nalbuphine. *J. Org. Chem.* **1984**, *49*, 2081–2082.
- Snow, R. J.; Baker, R.; Herbert, R. H.; Hunt, I. J.; Merchant, K. J.; Saunders, J. The synthesis of 5- and 6-substituted quinuclidine-3-carboxylic esters: intermediates for novel muscarinic ligands. *J. Chem. Soc., Perkin Trans. 1* **1991**, 409–420.
- Fürstner, A.; Leitner, A.; Méndez, M.; Krause, H. Iron-catalyzed cross-coupling reactions. *J. Am. Chem. Soc.* **2002**, *124*, 13856–13863.
- Hutchison, A. J.; Chenard, B. L.; Luke, G. P.; Li, G.; Ghosh, M.; Peterson, J. M.; Tarrant, J. G.; Doller, D. Substituted 1-Heteroaryl-4-Substituted Piperazine and Piperidine Analogues. Patent Application US2005/0239791, 2005.
- Rombouts, F. J. R.; De Borggraeve, W. M.; Delaere, D.; Froeyen, M.; Toppet, S. M.; Compennolle, F.; Hoornaert, G. J. Development of a functionalizable external β -turn mimic based on a cis-fused 1,7-naphthyridine scaffold. *Eur. J. Org. Chem.* **2003**, 1868–1878.
- Hartz, R. A.; Ahuja, V. T.; Arvanitis, A. G.; Rafalski, M.; Yue, E. W.; Denhart, D. J.; Schmitz, W. D.; Ditta, J. L.; Deskus, J. A.; Brenner, A. B.; Hobbs, F. W.; Payne, J.; Lelas, S.; Li, Y. W.; Molski, T. F.; Mattson, G. K.; Peng, Y.; Wong, H.; Grace, J. E.; Lentz, K. A.; Qian-Cutrone, J.; Zhuo, X. L.; Shu, Y. Z.; Lodge, N. J.; Zaczek, R.; Combs, A. P.; Olson, R. E.; Bronson, J. J.; Mattson, R. J.; Macor, J. E. Synthesis, structure–activity relationships, and in vivo evaluation of N^3 -phenylpyrazinones as novel corticotropin-releasing factor-1 (CRF₁) receptor antagonists. *J. Med. Chem.* **2009**, *52*, 4173–4191.
- Suginome, H.; Orito, K.; Yorita, K.; Ishikawa, M.; Shimoyama, N.; Sasaki, T. Photoinduced molecular transformations. 157. A new stereo- and regioselective synthesis of 2,6-diaryl-3,7-dioxabicyclo[3.3.0]octane ligands involving a β -scission of alkoxy radicals as the key step. New total syntheses of (±)-sesamin, (±)-eudesmin, and (±)-yangambin. *J. Org. Chem.* **1995**, *60*, 3052–3064.

- (41) Tsutsumi, H.; Tabuchi, S.; Minagawa, M.; Akahane, A. Pyrazine Derivatives and Pharmaceutical Use Thereof. Patent Application US2005/0222159, 2005.
- (42) Narsaiah, B.; Sivaprasad, A.; Venkataratnam, R. V. A novel synthetic route to 2-amino-3-cyano-4-trifluoromethyl-6-substituted pyridines. *J. Fluorine Chem.* **1994**, *67*, 87–90.
- (43) Kellogg, R. M.; Schaap, P.; Harper, E. T.; Wynberg, H. Acid-catalyzed brominations, deuteration, rearrangements, and debrominations of thiophenes under mild conditions. *J. Org. Chem.* **1968**, *33*, 2902–2909.
- (44) Wallace, D. J.; Chen, C.-Y. Cyclopropylboronic acid: synthesis and Suzuki cross-coupling reactions. *Tetrahedron Lett.* **2002**, *43*, 6987–6990.
- (45) Zulauf, A.; Mellah, M.; Guillot, R.; Schulz, E. Chromium-thiophene-salen-based polymers for heterogeneous asymmetric hetero-Diels–Alder reactions. *Eur. J. Org. Chem.* **2008**, 2118–2129.
- (46) Ertl, P.; Rohde, B.; Selzer, P. Fast calculation of molecular polar surface area as a sum of fragment-based contributions and its application to the prediction of drug transport properties. *J. Med. Chem.* **2000**, *43*, 3714–3717.